

Bulk-cone singularities & signatures of horizon formation in AdS/CFT

Veronika E Hubeny^Y, Hong Liu¹, and Mukund Rangamani^Y

^Y Centre for Particle Theory & Department of Mathematical Sciences,
Science Laboratories, South Road, Durham DH1 3LE, United Kingdom

¹ Center for Theoretical Physics, Massachusetts Institute of Technology,
Cambridge, Massachusetts, 02139, USA

February 18, 2019

Abstract

We discuss the relation between singularities of correlation functions and causal properties of the bulk spacetime in the context of the AdS/CFT correspondence. In particular, we argue that the boundary field theory correlation functions are singular when the insertion points are connected causally by a bulk null geodesic. This implies the existence of "bulk-cone singularities" in boundary theory correlation functions which lie inside the boundary light-cone. We exhibit the pattern of singularities in various asymptotically AdS spacetimes and argue that this pattern can be used to probe the bulk geometry. We apply this correspondence to the specific case of shell collapse in AdS/CFT and indicate a sharp feature in the boundary observables corresponding to black hole event horizon formation.

1 Introduction

The AdS/CFT correspondence, which relates quantum gravity in asymptotically Anti-de Sitter spacetimes to a non-gravitational gauge theory, is an invaluable window to understanding effects of gravity beyond the semi-classical approximation. In principle the correspondence provides a framework to address many long standing questions in quantum gravity, such as the nature of singularity resolution or issues relating to the information paradox. While much has been learnt in the past few years, the status of the dictionary between gravitational quantities and field theory observables is still at a somewhat rudimentary stage. This has been a stumbling block for exploiting the correspondence to its full power, especially in eliciting answers to off posed quantum gravitational questions.

In classical general relativity, concepts such as causal structure, event horizons, singularities, etc., play an important role in understanding the geometry of the spacetime manifold. In the semi-classical approximation these concepts are useful in understanding the dynamics of quantum fields in curved backgrounds. Given the AdS/CFT correspondence it is interesting to understand field theoretic encoding of these geometric concepts. Considering the central role played by geometry in classical general relativity, one naively expects them to have a well defined representation in the field theory.

For instance, consider the field theoretic representation of bulk causal structure. In the semi-classical limit, the bulk causal structure can be read off from the properties of correlation functions of quantum fields propagating on the spacetime manifold. For asymptotically AdS spacetimes the bulk correlation functions in turn determine (in some suitable scaling limit) the boundary correlation functions. Consistency within the correspondence requires therefore that the boundary correlation functions are compatible with the bulk causality constraints. This has been demonstrated to be true in many examples [1-4]. A crucial ingredient in most of these analyses has been to exploit the asymptotic AdS geometry where consistency is guaranteed by the symmetries in question.

The non-trivial aspect of the geometry that one would like to understand is the behaviour of the bulk causal structure deep in the interior of an asymptotically AdS spacetime. For example one can ask whether the presence of an event horizon in the spacetime has a non-trivial signature in the boundary. The zeroth order answer to this question, at least for eternal black holes in AdS spacetime, is that the dual field theory is in a thermal state.¹ So the presence of the horizon is encoded in a new scale for physics in the boundary theory, the thermal scale. However, this information hardly probes the causal structure in the vicinity of the horizon.

Furthermore, since the AdS/CFT correspondence is most fully understood in the Euclidean framework, questions pertaining to genuinely time-dependent processes in the bulk

¹This is true only for black holes whose horizon size is larger than the AdS scale.

and holographic duals thereof become much more subtle. For example, consider modelling a time dependent process, such as of black hole formation in the bulk, within the field theory. A more nuanced question, then, would be to ask whether there is any field theory information to be gained about the event horizon formation process. Phrased differently: can we see horizon formation directly in the gauge theory? Since in the bulk the event horizon forms at a sharply-localized event² (despite the fact that we need to know the full future evolution of the spacetime to actually find the horizon), we would expect that this will manifest itself in some correspondingly sharp feature in the gauge theory.

The conventional lore is that the UV/IR relation, which maps local regions in the interior of the bulk to non-local objects in the CFT, makes it hard to extract useful information about bulk geometry (cf., [5] for attempts to use UV/IR relation to extract information about the horizon). Given that the geometric scale associated with the horizon corresponds to the thermal scale for neutral black holes, it is hard to see how to extract a precise signal about the causal structure in the neighbourhood of the event horizon.

The clue comes from the progress made in the recent past in identifying the CFT signature of the black hole singularity [6,7]. In this case the field theoretic observables transcend the classical barrier of the event horizon to encode information of behind the horizon physics. The main observation of [6], which built on the original work of [8,9] was to use the intrinsic non-locality of the boundary correlation functions to identify signals of the singularity. The black hole singularity was identified to correspond to a particular ‘light-cone’ like singularity in the field theory correlation function.³ It has further been proposed that this technique can be exploited to understand physics behind the event horizon and in particular used to investigate aspects of stationary geometry within AdS/CFT [10]. The basic idea was to look at the bulk Green’s functions in a saddle approximation where they are dominated by geodesics and use the bulk computations to derive predictions for boundary correlation functions.

In the present work we argue that the horizon formation in gravitational collapse can be detected in the boundary theory by examining the structure of singularities of generic Lorentzian correlators. In particular, we show that a sharp horizon-formation time can be extracted from the pattern of singularities.

Our argument is based on a connection between null geodesics in the bulk spacetime and singularities in correlation functions of local operators evaluated in the state corresponding to

²In this work we consider spherically symmetric spacetimes. More generally, in non-spherical spacetimes the event horizon could form at a locus of events; our methods should generalise to these cases as well.

³The identification of the singularity in the strict large N limit is easiest when formulated in terms of momentum space correlators [7] as opposed to direct computation in position space where the singularity is not visible in the primary sheet of the correlator [6]. In particular, it was concluded in [7] that the signatures of the singularities go away when the rank of the boundary theory gauge group is finite, implying that the singularities are resolved in quantum gravity.

the bulk geometry.⁴ The basic idea is that CFT correlators will exhibit light-cone singularities when the points of operator insertion are connected by a null geodesic. The connection implies that CFT correlators in excited states have additional Lorentzian singularities inside the light cone, which we will call bulk-cone singularities. Usually CFT correlators exhibit light-cone singularities and the location of these is determined by the causal structure of the background spacetime on which the field theory lives. For a CFT living on $\mathbb{R} \times S^{d-1}$ these would be given by the conventional light cone of the Einstein static universe. Our main observation is that bulk causality, together with the dictionary between bulk Green's function and boundary correlation functions in the AdS/CFT context, necessitate additional bulk-cone singularities in the CFT correlators.

Armed with this relation we can ask how certain geometric structures are encoded in the boundary data. In addition to a black hole collapse geometry which motivated this study, we also look at the geometry of a star in AdS spacetime and the eternal black hole geometry. In all these cases, interesting details about the geometry and its causal structure that can be read off from the properties of the singularities in the CFT correlators. In fact, as has recently been shown in [11], the location of the boundary singularities can be used to reconstruct the complete bulk metric for a class of static, spherically symmetric spacetimes. Our analysis is carried out by explicitly studying geodesics in the bulk spacetime and using this to infer properties about correlation functions in strongly coupled gauge theories. While there are a few consistency checks we can establish in some simple cases, many of our results are predictions for strong coupling CFT correlation functions in certain excited states.

The plan of the paper is as follows: We begin in Section 2 by motivating our claim that Lorentzian AdS/CFT correspondence implies that correlation functions of local operators evaluated in excited states of the field theory exhibit light-cone singularities whenever the operator insertion points are connected by null geodesics through the bulk spacetime. We then confirm the relation between light-cone singularities and bulk null geodesics for vacuum correlators. Further, we generalize to excitations about vacuum state and obtain predictions for the singularities in the correlation functions from the behaviour of null geodesics. To demonstrate how sensitively the singularity pattern depends on the state, in Sections 3 and 4 we explicitly study the nature of the singularities and their implications for correlation functions in two scenarios: a generic excited state and a thermal state, which we model in the bulk by a star in AdS and an eternal black hole geometry, respectively. We devote Section 5 to our main example, the collapse of a black hole in AdS spacetime, and elicit from the geometry signatures of event horizon formation in the field theory. We conclude in Section 6 with a discussion. Finally, in the Appendices we present more detailed calculations pertaining to the various geometries considered (pure AdS, star in AdS, eternal Schwarzschild-AdS, Poincare patch, null shell collapse, and Vaidya-AdS).

⁴Spacetimes which are asymptotically AdS can be thought of as deformations of pure AdS by normalizable modes in the supergravity description. In field theory terms this corresponds to a generic excited state obtained by acting on the CFT vacuum with the appropriate operator.

2 Null geodesics and boundary singularities

In this section we motivate a simple relation between singularities of the boundary correlation functions and null geodesics in the bulk spacetime. The main idea is to exploit the AdS/CFT dictionary for evaluating strong coupling correlation functions in the CFT using bulk Green's functions. Since the bulk Green's functions are sensitive to the bulk causal structure we expect that the properties of the bulk light cone to be directly visible in the boundary correlation functions.

A short word on notation: for convenience, we will denote the $d+1$ dimensional bulk spacetime by M and its d dimensional boundary by $@M$. Further, we use labels $x; y$ etc., for points on the boundary $@M$ and r to denote the radial coordinate normal to $@M$.

2.1 General argument

The AdS/CFT correspondence gives us a precise map relating string theory (or its low energy supergravity limit) on M with a field theory living on the boundary $@M$ of M . To be precise, in the low energy supergravity approximation of the bulk theory (which is good as long as we choose the 't Hooft coupling λ and the rank of the gauge group N on the boundary to be large, i.e., $\lambda \gg 1$ and $N \gg 1$) we can obtain the boundary correlation function $G(x; x^0)$ from the bulk propagator $G(x; r; x^0; r^0)$ of the corresponding field by taking both end points to the boundary. More precisely,

$$G(x; x^0) = 2 \lim_{r \rightarrow 1, r^0 \rightarrow 1} (rr^0) G(x; r; x^0; r^0); \quad (2.1)$$

where G is the free field theory propagator for the corresponding bulk field. Focussing on the simple case of local gauge invariant operators $O(x)$ of conformal dimension Δ in $@M$ which are dual to free scalar fields parameterized by mass m in the bulk, in (2.1) we have

$$= \frac{d}{2} + \frac{\Delta}{2}; \quad = \frac{r}{m^2 + \frac{d^2}{4}}; \quad (2.2)$$

where we have set the curvature radius of AdS to be 1. Note that by choosing the asymptotic AdS time to coincide with the boundary time, one ensures that time ordering chosen for the bulk propagator G carries over to the boundary correlator in the limiting procedure. In what follows we will consider Feynman propagators.

That the limit in (2.1) is well-defined for an asymptotically AdS spacetime can be seen as follows. Upon fixing $(x^0; r^0)$, $G(x; r; x^0; r^0)$ is a normalizable solution of the free bulk wave equation on M . This implies for an asymptotically AdS spacetime

$$G(x; r; x^0; r^0) \sim r^{-\Delta}; \quad r \rightarrow 1; \quad (2.3)$$

Similarly,

$$G(x; r; x^0; r^0) \sim r^{\Delta}; \quad r^0 \rightarrow 1; \quad (2.4)$$

Thus for generic boundary points x and x^0 , the limit (2.1) is well defined and yields a regular $G(x; x^0)$. However, if x and x^0 are connected by a null geodesic, (2.3) and (2.4) could break down, in which case one expects

$$\lim_{r \rightarrow r^0} G(x; r; x^0; r^0) \neq 0 : \quad (2.5)$$

A naive application of (2.1) will yield a divergent answer as the limit is not well-defined.

In order to obtain explicitly the singular behavior of $G(x; x^0)$ has to work with a suitably regularized expression. To this end one can first consider some x^0 lying in a small neighborhood of x^0 in the boundary. If x^0 is not connected to x by null geodesics, (2.1) can be straightforwardly applied to obtain $G(x; x^0)$. One can then take $x^0 \rightarrow x^0$ to obtain the desired correlator $G(x; x^0)$.

We will now motivate the above discussion in a slightly different perspective using the geodesic approximation to $G(x; r; x^0; r^0)$. For this purpose, we will take m large⁵ so that $m \gg 1$. To consider the limit (2.1), we put the boundary ∂M at a cut-off surface $r = r^0 = r^0 + \epsilon$, on which (for an asymptotically AdS geometry) the induced metric can be approximated as

$$ds^2 = -dt^2 + ds_{\text{bd}}^2 \quad (2.6)$$

where ds_{bd}^2 denotes the metric on the boundary ∂M .

Consider points $A = (x; t)$ and $B = (x^0; t)$ on the cut-off surface, which are spacelike separated. In the large m limit, one expects that the saddle point approximation is valid. Denoting by $d(A; B)$ the proper distance between two (spacelike separated) points in M we have

$$G(A; B) \sim e^{-m d(A; B)} \sim e^{-2m \log \frac{d(A; B)}{2}} ; \quad (2.7)$$

where we used the fact that as $m \gg 1$, the proper distance $d(A; B) \sim 2 \log \frac{d(A; B)}{2} + \dots$ in asymptotically AdS spacetimes. Note that (2.7) is consistent with (2.3) and (2.4) and hence makes sure that the limit (2.1) is well defined.⁶

Now suppose that there is a null geodesic connecting A and B (in this case $d(A; B) = 0$ and $G(A; B) \sim O(1)$). As suggested above we consider points $C = (x^0; t)$ in a small neighborhood of B , for which

$$d(A; C) \sim \log \left[\frac{2}{\epsilon} \frac{d(x; x^0)}{2} \right] \quad (2.8)$$

where x is the proper distance between x and x^0 on the boundary (i.e., in terms of metric ds_{bd}^2 in (2.6) on ∂M). Plugging (2.8) into (2.7) and then taking the limit as suggested in (2.1), we have

$$G(x; x^0) \sim \frac{2m}{(\frac{d(x; x^0)}{2})^m} ; \quad x^0 \rightarrow x^0 : \quad (2.9)$$

⁵The relation between null geodesics and singularities of $G(x; x^0)$ does not require taking m large.

⁶For generic timelike separated points $A; B$ on ∂M , we also expect (2.7) to be true based on analytic continuation from spacelike separated points. Note that in the pure AdS, G is a function of the proper distance $d(A; B)$ which can be analytically continued in the complex plane to timelike separation.

To summarize, we have argued that a boundary correlation function $G(x; x^0) = \langle \mathcal{O}(x) \mathcal{O}(x^0) \rangle$ is singular if and only if⁷ there exist null geodesics connecting x and x^0 . Our argument is not completely rigorous and we discuss potential loopholes below. This proposal can be checked in simple examples in which one can work out the boundary $G(x; x^0)$ explicitly, like global pure AdS, Poincare patch and the BTZ black holes (see appendices).

2.2 Types of null geodesics and causal structure

In this subsection we discuss the location of the singularities in $G(x; x^0)$ and structure of null geodesics. For this purpose, let us $x \rightarrow x^0$ and consider those x^0 which are connected to x by null geodesics. The null geodesics can be divided into two types: those lying entirely in the boundary (type A) and those lying in the bulk except for their end points (type B). Type A geodesics are simply null geodesics of the boundary theory and define the light cone of the CFT. For points x and x^0 connected by Type A null geodesics, $G(x; x^0)$ has the standard light-cone singularities. Type B null geodesics are more interesting and we now discuss them in some detail.

In pure global AdS (where the boundary is $\mathbb{R} \times S^{d-1}$), all Type B null geodesics connect the antipodal points on S^{d-1} . The points in question are given by $(t_i; \vec{x}_i)$ and $(t_o; \vec{x}_o)$, with $t_o - t_i = R_{\text{AdS}}$ and $\vec{x}_o = -\vec{x}_i$ denote points which are antipodal on the S^{d-1} . Note that the (boundary) time separation $t_o - t_i = R_{\text{AdS}}$ needed for the geodesic to traverse the bulk is exactly the same as that of a Type A null geodesic connecting the antipodal points only in pure AdS spacetime; the former becomes longer for general asymptotically AdS spacetimes. Further details on geodesics in AdS, both analytic and pictorial, appear in Appendix A.

Since in the case of pure AdS the end points of the Type B null geodesics already coincide with the boundary light cone, they do not give rise to additional singularities in the boundary correlation functions. It is easy to verify that the behaviour of null geodesics in AdS is consistent with the singularity properties of boundary correlation functions. The boundary correlators in question are two-point functions in the CFT vacuum of primary operators of dimension Δ which for a d -dimensional CFT on $\mathbb{R} \times S^{d-1}$ are given by

$$\langle \mathcal{O}(t; \vec{x}) \mathcal{O}(t^0; \vec{x}^0) \rangle \sim \frac{1}{(\cos(t - t^0) - \cos(\vec{x} - \vec{x}^0))^\Delta}; \quad (2.10)$$

The singularities of the correlation function (2.10) are given by $t = t^0$ with $\vec{x} = \vec{x}^0$ etc., which coincide with the light cone of the boundary manifold.

In a perturbed AdS spacetime, the end points of Type B geodesics in general do not coincide with the light cone of the boundary manifold. They will therefore give rise to

⁷While we have explicitly shown that bulk null geodesics lead to new singularities in boundary correlation functions, our arguments indicate that the converse should also be true. This is equivalent to the statement that (2.5) is true only for points connected by null geodesics.

additional singularities in the boundary correlation functions. We will call such singularities bulk-cone singularities. An interesting feature of asymptotically AdS spacetimes is that there exists a lower bound on the ‘time delay’ experienced by geodesics exploring the bulk spacetime. In a situation where the bulk manifold M with a timelike conformal boundary ∂M satisfies the null energy condition, the null generic condition, and strong causality and compactness, it has been proven by Gao and Wald [3] that the end points x^0 of Type B geodesics always lie inside the light cone of the boundary manifold, i.e., x^0 and x are timelike separated. This implies that any generic perturbation of AdS (satisfying the conditions mentioned) will produce a time delay of null geodesics relative to pure AdS. For example, imagine a state corresponding to a thermal gas in AdS at some internal mass density ρ . Then a radial geodesic will arrive to the anti-podal point of the boundary after a time t which increases monotonically with increasing ρ .

This implies that correlation functions in some excited states⁸ of the theory will have additional Lorentzian singularities inside the light cone. We also note that it can be checked explicitly that for backgrounds with non-compact boundary, Type B null geodesics do not exist (for a proof of the statement see Appendix D). Thus additional singularities appear to arise only for CFTs on compact spaces.

While the theorem of Gao and Wald only applies to asymptotically AdS spacetime satisfying the conditions stated above, from the causality of the boundary theory one would like to conclude that the end points of Type B null geodesics should always lie inside the light cone of the boundary for any asymptotically AdS background with a deld theory dual. Otherwise it would imply that one can set up a special state in the deld theory to transmit signals faster than the speed of light (see also [12]).

To conclude this section let us comment on a potential loophole in our argument. Our connection between null geodesics and singularities of boundary correlation functions is based on the validity of (2.5) for any two points connected by a null geodesic. While this assumption is consistent with our general understanding of quantum deld theory in a curved spacetime, we do not have a rigorous proof of the statement.⁹ Also note that one should distinguish be-

⁸In order to have non-negligible back reaction on the bulk metric, the ADM mass M of the perturbation should satisfy $G_N M \sim O(1)$. This implies that the corresponding excited state in boundary theory should have energy of order $O(N^2)$. In the following discussion, by generic excited states, we mean generic states of such energies.

⁹For example, in a semi-classical approximation to the propagator, one may consider the following scenario: In general, the end points of a null geodesic can be shared by other spacelike and/or timelike geodesics. If the propagator is given by summing over all geodesics, then the null geodesic clearly dominates. However, there might be a situation that path integration contours for the propagator cannot be deformed to the saddle point corresponding to the null geodesic. Then the null geodesic will not contribute to the propagator, even though it naively dominates. A analogous phenomenon was encountered in [6] for a spacelike (almost null) geodesic bouncing off a black hole singularity; though it is not clear whether this contingency will ever arise for strictly null geodesics. Given that one can send light signals following null geodesics, one

tween points which can be connected by a null geodesic and those points which the geodesics connecting them only approach null. In the latter case, when there does not exist a null geodesic which connects two points, our argument does not directly apply. We will elaborate more on this when discussing the gravitational collapse background in Section 5.

3 Static asymptotically AdS geometries

We now turn to applying the results of Section 2 to static spacetimes. A trivial example where our relations can be verified is of course the empty AdS spacetime which we have already commented on. We now turn to consider geometries which are deformations of AdS, with a free parameter such that pure AdS is retrieved in a particular limit of this parameter. We will first consider situations with sufficient symmetries to simplify the analysis before turning to more complicated examples. For concreteness, we will work in 5 dimensions, i.e., take the spacetime to be asymptotically AdS₅ (time is a S⁵ which will not play any role).

3.1 Geometries of stars in AdS

As our first nontrivial example, we will take our spacetime to be static and spherically symmetric, and to make things even simpler, we will take the matter content to be that of a self-gravitating gas of radiation. The symmetries imply the corresponding stress tensor is that of a perfect fluid; radiation equation of state which makes the stress tensor traceless, i.e.,

$$T_{ab} = \rho(r) u_a u_b + P(r) (g_{ab} + u_a u_b); \quad P = \frac{1}{4} \rho \quad (3.1)$$

where u^a is a co-moving gas 4-velocity, and $\rho(r), P(r)$ are density and pressure. Since the radiation will be confined by the AdS potential, we will refer to this configuration as a "star" in AdS. The metric can be obtained by solving the Einstein's equations with negative cosmological constant and the requisite stress tensor, as discussed in detail in Appendix B. Here we summarize the main results.

The metric can be written in the form :

$$ds^2 = -f(r) dt^2 + h(r) dr^2 + r^2 d\Omega_3^2 \quad (3.2)$$

with

$$h(r) = r^2 + 1 - \frac{m(r)}{r^2} \quad (3.3)$$

and

$$f(r) = \frac{1}{r^2} \quad (3.4)$$

might be able to argue a null geodesic should always contribute to a propagator.

where the mass function $m(r)$ is defined in terms of an integral of the density $\rho(r)$,

$$m(r) = \frac{2}{3} \int_0^r \rho(r') r'^3 dr' \quad (3.5)$$

and ρ_1 is the coefficient of the leading fall-off of $\rho(r)$, determined by $\rho(r) \sim \rho_1 r^{-5}$ as $r \rightarrow \infty$. The field equations specify the system of coupled first order ODEs which $m(r)$ and $\rho(r)$ must satisfy:

$$m'(r) = \frac{2}{3} \rho(r) r^3 \quad (3.6)$$

$$\rho'(r) = -\frac{5}{r} \rho(r) - \frac{r^2 + \frac{m(r)}{r^2} + \frac{1}{12} \rho(r) r^2}{r^2 + 1 - \frac{m(r)}{r^2}} \quad (3.7)$$

with boundary conditions $m(0) = 0$ and $\rho(0) = \rho_0$, where ρ_0 is a free parameter of the configuration, specifying the internal density of the gas. Thus the geometries are parameterized by a single parameter ρ_0 , with pure AdS retrieved in the $\rho_0 = 0$ case.

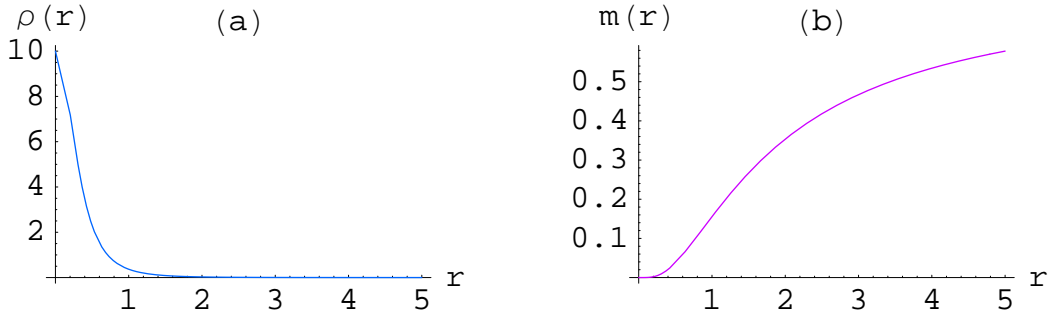


Fig. 1: Density and mass functions for the "star" geometry, where the central density is set to $\rho_0 = 10$.

From (3.6) and (3.7) we find the following asymptotic behavior for $m(r)$ and $\rho(r)$

$$r \rightarrow \infty : \quad \rho(r) \sim \frac{1}{r^5} \left(1 - \frac{5}{2r^2} + \frac{5(4M+7)}{8r^4} + \dots \right); \quad (3.8)$$

$$m(r) \sim M - \frac{1}{r} + \dots \quad (3.9)$$

$$r \rightarrow 0 : \quad \rho(r) \sim \rho_0 + O(r^2); \quad m(r) \sim \frac{\rho_0}{6} r^4 + O(r^6) \quad (3.10)$$

where ρ_1 and M (M is proportional to ADM mass) are constants which are determined by ρ_0 . Using (3.3) and (3.4) we also find that

$$r \rightarrow \infty : \quad f(r) \sim r^2 + 1 - \frac{M}{r^2} + \dots \quad h(r) \sim r^2 + 1 - \frac{M}{r^2} + \dots \quad (3.11)$$

$$r \rightarrow 0 : \quad f(r) \sim \frac{1}{r^{\frac{2}{5}}} + O(r^2); \quad h(r) \sim 1 + O(r^2) \quad (3.12)$$

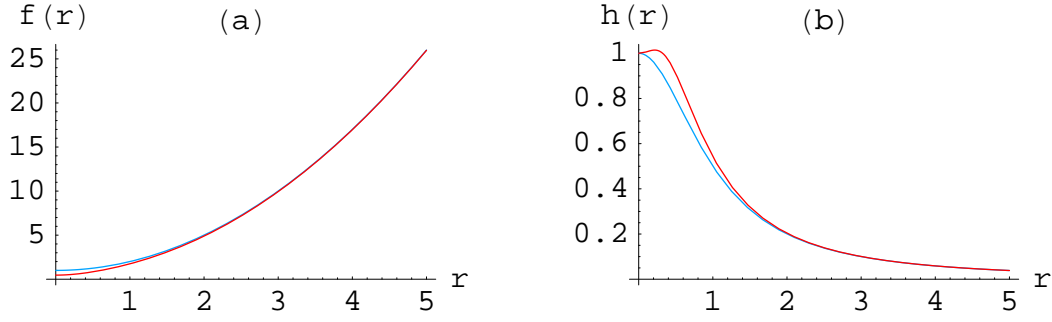


Fig. 2: Metric functions for the "star" geometry with central density $\rho_0 = 10$ (red curves), and for comparison corresponding metric functions in the pure AdS geometry (blue curves; $f(r)$ is the higher and $h(r)$ is the lower of the two curves).

One can readily solve the full equations (3.6) and (3.7) numerically. Fig.1 shows the density and mass functions for the internal density $\rho_0 = 10$.

The metric functions are plotted in Fig.2, again for the same set-up as in Fig.1. For comparison we also plot the corresponding metric coefficients for pure AdS; as we would expect, the metric does approach that of AdS as the density becomes small.

3.2 Geodesics in the star AdS geometry

We will now turn to the properties of bulk null geodesics (Type B) in the star geometry. Staticity and spherical symmetry implies that E (energy) and J (angular momentum) are conserved along any geodesic and hence we will parameterize the geodesics by these quantities. The equations for null geodesics are:

$$\dot{t} = \frac{1}{f(r)}; \quad \dot{r} = \frac{1}{r^2}; \quad \text{and} \quad f(r)h(r)\dot{r}^2 = -V(r); \quad (3.13)$$

where

$$V(r) = \frac{f(r)}{r^2}; \quad \frac{E}{J} \quad (3.14)$$

and the dot denotes differentiation with respect to the affine parameter along the geodesic. For null geodesics the absence of scale implies that the relevant parameter is the ratio $E=J$. Useful quantities for figuring out which points on the boundary are connected by null geodesics are the temporal and angular separation of the geodesic endpoints, which we denote by Δt and $\Delta \phi$, respectively. Since we have a numerical solution for the metric, we have to integrate the geodesic equations numerically to find the desired properties.

Consider first radial null geodesics, which we expect will emerge at a later time than the corresponding geodesic in pure AdS, consistent with the theorem of [3]. Denoting this time

by t_0 , we have

$$t_0 = 2 \int_0^z \frac{h(r)}{f(r)} dr \quad (3.15)$$

For a star geometry with central density $\rho_0 = 10$, we find numerically that $t_0 = 3.696$,

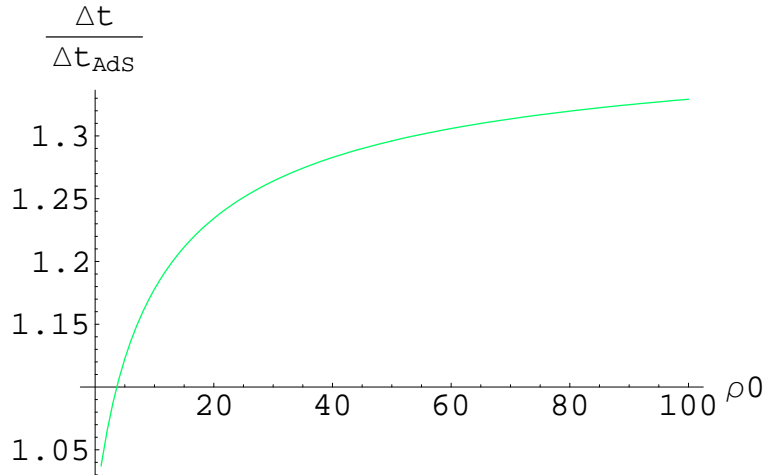


Fig. 3: Time delay for radial null geodesics through star in AdS, as a function of the star's internal density ρ_0 .

which is 1.177 times longer than in pure AdS. Fig.3 exhibits the dependence of this time delay on the value of ρ_0 . We see that while the time delay increases monotonically with increasing density, it does so more and more slowly.¹⁰

Now let us consider null geodesics with nonzero angular momentum. (Appendix B further explores non-radial spacelike geodesics.) In Fig.4, we show null geodesics projected onto a spatial (constant t) slice (left) and the $t-r$ plane (right). Not surprisingly, the star has a focusing effect on the geodesics. The important point to note is that now, unlike the pure AdS case, there is a finite spread of the t and r endpoint values the null geodesics can take. More specifically, because of the attractive nature of the star's gravitational potential, the small angular momentum ($J=E-1$) geodesics 'overshoot' in terms of angular separation, and at the same time they experience some time delay, which means that both t and r increase. However, this effect does not keep increasing monotonically with increasing angular momentum, because the further from the origin the geodesics penetrate, the less effect of the star they feel. In the high angular momentum limit ($J=E-1$), the geodesics hug the boundary and consequently behave just as the corresponding geodesics in pure AdS.

¹⁰The intuitive reason for t_0 not increasing more rapidly with ρ_0 is that the larger the internal density ρ_0 , the faster the density function $\rho(r)$ falls off, in such a way as to keep the total mass M bounded, as discussed in Appendix B. Numerically we find that t_0 appears to be bounded as $\rho_0 \rightarrow \infty$.

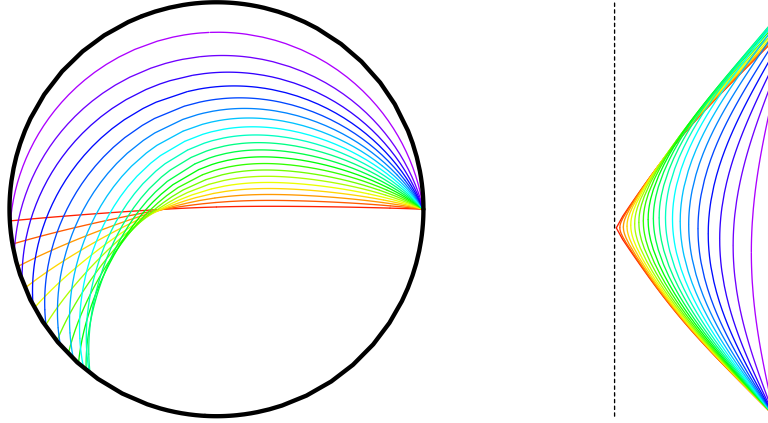


Fig. 4: Null geodesics in star with $\rho_0 = 10$ in AdS, projected onto a constant t slice and the $t-r$ plane, for varying angular momentum to energy ratio ($E = 10$ and $J = 0; 1; \dots; 10$). On the left, the bold circle corresponds to the AdS boundary, whereas on the right, the dashed vertical line corresponds to the origin $r = 0$ and the bold vertical line to the boundary at $\tan r = \frac{1}{2}$. The range of t plotted is $(0; 1; 1 - t_0)$. (Analogous plots with larger ρ_0 appear in Fig.19 of Appendix B.)

To illustrate explicitly how the endpoints of these various geodesics compare, Fig.5 summarizes the behaviour of t and r' for the various geodesics. In (a), where the endpoints are plotted for small internal densities, $\rho_0 = 1; \dots; 10$, we see that the effect of overshooting becomes more pronounced the higher ρ_0 is. In (b), where $\rho_0 = 10; \dots; 100$, we illustrate that the effect however remains bounded even for high internal densities. (We have verified this numerically for $\rho_0 \cdot 10^{18}$.) Note that the t intercept for each curve can be read off already from Fig.3.

The boundedness of t implies one of the interesting features for the star geometries, namely the absence of null geodesics orbiting the star. In fact, one can obtain this result more directly, as follows: From (3.13) we see that in order to have null geodesics at fixed radial distance from the star, i.e., $r(\lambda) = \text{constant}$, we require that $g^{tt} V(r) = 0$ and $\frac{d}{dr} V(r) = 0$. It is easy to show numerically that these conditions are never satisfied for the star geometries.¹¹ As we will argue below, this absence of circular orbits around the star leads to marked differences in the behaviour of singularities for correlation functions in the pure state corresponding to the star and in thermal density matrix represented by an eternal black hole geometry. In particular, in the star case, the spread of the geodesic endpoints remains bounded, unlike for the black hole case which has a circular orbit.

¹¹The two conditions can be distilled into a necessary condition for circular photon orbits; defining $Q(r) = \frac{1}{12} (r) r^2 + 2 \frac{m(r)}{r^2}$ we need $Q(r_0) = 1$ at some $r = r_0$. We find that $Q(r) < 0.6$ for all r irrespective of the internal density ρ_0 .

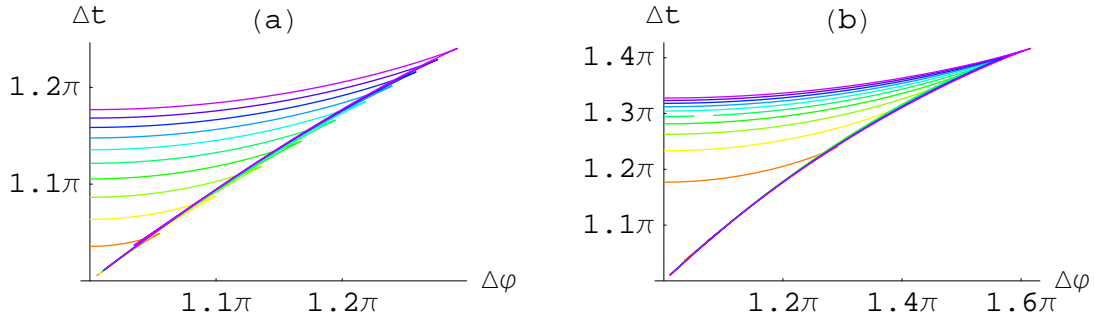


Fig. 5: Endpoints of null geodesics in the AdS geometry of star with (a) $\rho_0 = 1; 2; \dots; 10$ and (b) $\rho_0 = 10; 20; \dots; 100$. Each curve is plotted by varying $\theta = \frac{E}{J}$. The top of the curves corresponds to big values of θ ; in fact, one can easily show that the slope of each curve (as a function of θ) is given by $1 = \dots$.

The essential points relating to null geodesics in the star background can be summarized as follows:

The radial null geodesics which go through the bulk geometry emerge at the antipodal point on the sphere ($\theta' = \pi$) at a later time than in pure AdS ($t > \dots$). The time delay is a monotonic function of the internal density ρ_0 .

Null geodesics with angular momentum exhibit both a time delay as well as a shift in θ' . For small angular momentum, both t and θ' increase with increasing angular momentum, whereas for large angular momentum they decrease to match with the AdS value $t = \theta' = \dots$ when $J = E$. While this effect increases with increasing ρ_0 , t and θ' remain bounded for arbitrary ρ_0 .

There are no null geodesics at fixed value of the radial coordinate i.e., the star spacetime does not admit circular photon orbits.

We stress that since the endpoints of the null geodesics indicate the location of a singularity in the corresponding correlation function as discussed above, the data of Fig.5 is in principle easily extractible from the gauge theory. This demonstrates how from the gauge theory we can read off the details of the geometry deep inside the bulk. In other words, just by looking at the spread of the endpoints of the null geodesics, we can distinguish the star from a small black hole (as demonstrated below) or other configurations of the same mass in AdS. Note that this is rather different method of extraction of details of deep IR in the bulk from that employed in [13]: the latter considered one-point functions, whereas here we make explicit use of the nonlocal nature of the two-point functions.

3.3 Field theory signature of excited AdS geometries

We now turn to a brief analysis of the star geometry from a field theory perspective. By construction we have an asymptotically AdS geometry which is static and spherically symmetric. While we have modeled the star by an effective equation of state, it is easy to see that similar solutions can be obtained in gauged supergravity theories. In any event the geometries in question correspond to normalizable deformations of the AdS vacuum, implying that they are dual to states in the field theory. In particular, these states should be eigenstates of the CFT Hamiltonian (since they are static). One can therefore use the state operator correspondence in the CFT to map the state into an operator insertion; for convenience we will call the state of the star $|\text{star}\rangle$ and the corresponding operator O i.e., $|\text{star}\rangle = O|0\rangle$. Note that to obtain a geometry with spherical symmetry we would need to smear the operator insertion O on the boundary S^3 making it effectively non-local.

One of the interesting questions that we will be unable to provide a concrete answer for is the precise description of the state $|\text{star}\rangle$ in the field theory. From general arguments it is clear that the operator O has dimension of $O(N^2)$ in the field theory.¹² In order to ascertain the precise state we need more information than the one point function of the stress tensor (which is of course given by the leading fall-off in the metric). However, it is clear that on physical grounds such states ought to be constructible in the field theory and we will proceed with the assumption that O is a bona fide operator in the field theory.

Our analysis of geodesics in the star spacetime can be rephrased in light of the discussion in Section 2 as predictions for new ‘light-cone’ singularities in the boundary correlators in the state $|\text{star}\rangle$. The later arrival at the boundary of radial null geodesics consistent indicates that correlation functions of generic operators O in the field theory, $\langle \text{star} | O(x) O(y) | \text{star} \rangle$ will have singularities at $t' = t$ and t' given by the appropriate time delay. Similarly, the implication of bulk Type B geodesics with angular momentum is that we will have light-cone singularities in field theory correlators at operator insertion points $x; y$ such that $t_x - t_y = t$ and $x - y = t'$ with t and t' given by the geodesic analysis.

While we have emphasized the results here as predictions for the gauge theory correlation functions in an excited state at strong coupling, we believe that some of these predictions can be tested. For instance, one can consider the $l=2$ BPS states in $N = 4$ SYM. The geometries dual to these states are explicitly constructed in [14]. Within this class of geometries one can focus on those which are asymptotically AdS and calculate the bulk prediction for the light-cone singularities using the nature of bulk geodesics. To compare with the field theory result we need to know the behavior of four point functions, which can be analyzed in large N perturbation theory (at weak coupling) by taking the probe operators to also be chiral primary. We hope to report on this in the near future.

¹²This is because of the state being dual to a configuration of finite ADM mass M and the fact that the bulk Newton’s constant scales like N^{-2} .

4 Eternal black holes in AdS

In the previous section we discussed the behaviour of geodesics in spacetimes which are deformations of AdS, focussing on globally static geometries. We will now consider spacetimes such as the eternal Schwarzschild-AdS black hole which is causally nontrivial and not globally static. In this case we know that a large Schwarzschild-AdS black hole corresponds to a thermal state in the field theory. The analysis of geodesics will lead to interesting signatures of the black hole geometry which will be visible in thermal correlation functions.

4.1 Schwarzschild-AdS black hole: Structure of spacelike and null geodesics

We will first describe the structure of null and spacelike geodesics in an AdS black hole background. Again focusing attention on 5-dimensional AdS, the black hole metric is given by

$$ds^2 = -f(r) dt^2 + \frac{1}{f(r)} dr^2 + r^2 d\Omega_3^2 \quad (4.1)$$

with

$$f(r) = r^2 + 1 - \frac{r_+^4}{r^2} \quad (4.2)$$

The mass of the black hole is proportional to r_+^4 , and correspondingly the horizon radius r_+ and the inverse Hawking temperature are given by¹³

$$r_+^2 = \frac{\sqrt{1+4} - 1}{2}; \quad T = \frac{2}{2r_+^2 + 1} \quad (4.3)$$

The equations for general geodesics are given as:

$$\dot{t} = \frac{1}{f(r)}; \quad \dot{r} = \frac{1}{r^2}; \quad \text{and} \quad \dot{\underline{x}}^2 = 2 - V_{\text{eff}}(r); \quad (4.4)$$

where

$$V_{\text{eff}}(r) = \frac{1}{J^2} f(r) + \frac{f(r)}{r^2} \quad (4.5)$$

and $J = 1; 0; \text{ or } -1$ for spacelike, null, or timelike geodesics, respectively, and the dot denotes differentiation with respect to the affine parameter along the geodesic.

Null geodesics in the black hole background ($J = 0$) are parameterized by the ratio $\frac{t}{r} = \frac{E}{J}$. Once again we will be interested to know which points are connected by bulk null geodesics and we will quantify this in terms of $(t(\cdot)); (r(\cdot))$. The radial equation is easy to interpret as a classical particle with energy E^2 moving in a potential $V_{\text{eff}}(r) = \frac{f(r)}{r^2}$ (see Fig. 6). $V_{\text{eff}}(r)$ has a maximum at $r_m^2 = 2$ with a value $V_{\text{eff}}(r_m) = 1 + \frac{1}{4}$ and as $r \rightarrow 1$, $V_{\text{eff}} \rightarrow 1$. The null geodesics connecting boundary points are:

¹³Note that to describe a big black hole we need $r_+ \geq \frac{3}{4}$. Further, for the temperature of the system to be high enough so that the big black hole dominates the thermal ensemble, we require $r_+ \geq 2$, which corresponds to $T = \frac{1}{2} \leq \frac{3}{2}$. For illustration, we often use an example with $r_+ = 1$ below.

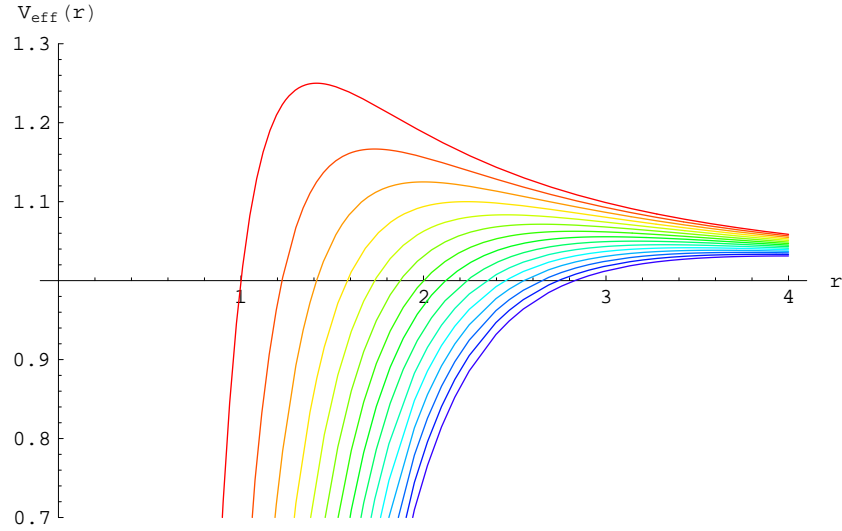


Fig. 6: The plot for $V_{\text{eff}}(r) = f(r) = r^2$ for $2 < \beta < 1.5; 2; \dots; 7.5; 8g$.

1. Geodesics with $\beta = 1$, i.e., $E = J$, stay at constant $r = 1$; these are null geodesics of the boundary manifold (Type A).
2. The null geodesics which pass into the bulk and come back to the boundary (Type B) exist only for $\beta > 1; \beta_0$, where

$$\beta_0^2 = V_{\text{eff}}(r_m) = 1 + \frac{1}{4} \quad (4.6)$$

As $\beta \rightarrow 1$, we find that $(t; r) \rightarrow (0; 1)$. It is also clear from Fig. 6 that as $\beta \rightarrow \beta_0$, $t(\beta)$ and $r(\beta)$ should go to infinity since it takes infinite parameter time to reach the turning point.¹⁴ One can further check that

$$\frac{dt}{d\beta} = \frac{dr}{d\beta} \quad \Rightarrow \quad \frac{dr}{dt} = r(\beta) \quad (4.7)$$

From this we conclude that as $\beta \rightarrow \beta_0$,

$$t(\beta) \sim \frac{1}{\beta - \beta_0} \quad (4.8)$$

Note that since $\beta_0 > 1$, the above equation implies $t < r$. This remains true for general values of $\beta > \beta_0$ as is clear from Fig. 7, which is a parametric plot of $r(\beta)$ vs $t(\beta)$ by varying β . Note that since r is periodic, there is no violation of causality here.

¹⁴Or said differently, as $\beta \rightarrow \beta_0$, the geodesic can go around the circular orbit at $r_m = \sqrt{\frac{\beta - \beta_0}{2}}$ many times before re-escaping to the boundary.

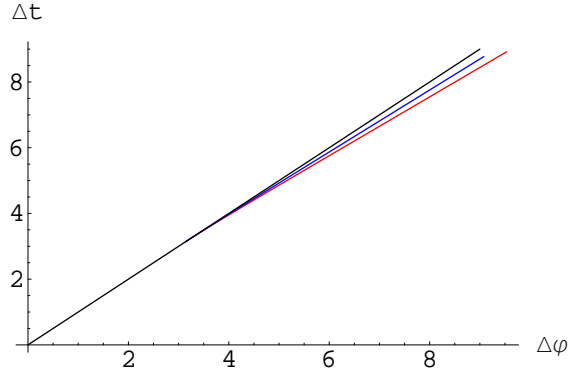


Fig. 7: End points of null geodesics in a black hole background. The black line is $t = \tau$, which is the set of end points of boundary null geodesics. The blue and red curves give the end points of bulk null geodesics for a black hole with $\alpha = 2$ and $\beta = 1$, respectively. It is obtained by varying $\beta = 2(1; \beta_0)$. As $\beta \rightarrow 1$, $(t; \tau) \rightarrow (\beta; \beta)$ and as $\beta \rightarrow \beta_0$, t and τ approach infinity with their ratio given by $1 = \beta_0$. Note that $\tau(\beta) > t(\beta)$ for $\beta = 2(1; \beta_0)$.

In order to better understand the set of boundary points that can be connected through the bulk, we should also look at spacelike geodesics, which are discussed in detail in Appendix C.

4.2 New singularities for thermal YM theories on S^3

We now consider gauge theory implications of the null geodesics in the black hole background. As discussed in Section 2, we will assume that null geodesics lead to the singularities of boundary correlation functions.

At a spatial point $\tau = \tau_0$, boundary null geodesics will give rise to singularities at

$$t = \tau_0; \tau_0 + 2; \tau_0 + 4; \dots \quad (4.9)$$

These are singularities of vacuum correlation functions and we expect they survive at finite temperature as well. Type B null geodesics which go into the bulk will give rise to new singularities at

$$t_1 = \tau_0 + 2 b_1(\tau_0); t_2 = t_1 + 2 b_2(\tau_0); \dots; t_n = t_{n-1} + 2 b_n(\tau_0); \dots \quad (4.10)$$

where $t_n; n = 1; 2; \dots$ are obtained by the intersection of the red line with vertical lines $\tau = 2n + \tau_0$ in Fig.7. Here $b_n(\tau_0)$ is some number lying between $1 = \beta_0$ and 1 and is smaller than 1. As n becomes large,

$$b_n(\tau_0) \rightarrow \frac{1}{\beta_0} = \frac{1}{1 + \frac{1}{4}} \quad (4.11)$$

independent of the value of r_0 . The locations of these singularities are temperature-dependent, since r_0 and b_n depend on the temperature of the system (through β). Since all b_n are smaller than 1, the singularities in (4.10) are generically distinct¹⁵ from those in (4.9). Note as we increase the temperature of the system (i.e., increase the black hole mass), $r_0 \rightarrow 1$ and the two sets of singularities merge in the $r_0 \rightarrow 1$ limit. In the high temperature limit, S^3 effectively decompactifies to R^3 , and as we discussed earlier there are no bulk null geodesics in this limit (see Appendix D).

Since "new" singularities arise from null geodesics which go into the bulk, they encode information regarding the bulk geometry. That singularities exist for $r_0 \rightarrow 1$ is a reflection of the existence of a (unstable) circular orbit at $r_n = \sqrt{\frac{p}{2}}$ in the bulk geometry. The time difference $t_n - t_{n-1}$ between nearby singularities for n large is simply given by the time that it takes a null geodesic to transverse the circular orbit (which is $2\pi = \beta$). More generally, denoting the locations of the singularities by the curve $t(r)$, from the second equation of (4.7) it follows that the slope $\frac{dt}{dr}$ gives $1 = \frac{J}{E} = J/E$ of the corresponding bulk geodesic.

Also note that in cases where the bulk geometry deviates from that of the Schwarzschild-AdS geometry in the vicinity of the horizon, such as the smooth microstate geometries discussed in the context of D1-D5 systems (cf., [15,16] for reviews and references), the gauge theory should in principle be able to detect even slight deviations which cause a slight shift in the radius of the null circular orbit. This is facilitated by the fact that the slope $\frac{dt}{dr}$ can be measured arbitrarily precisely for large enough separations t and r .

Our conclusion above was obtained in the supergravity limit, i.e., large N and large limit. It would be interesting to understand whether the "new singularities" at finite temperature arise when one departs away from the limit. In particular, it would be interesting if one could find independent arguments for their existence in the gauge theory.

5 Horizon formation from gauge theories

In the preceding sections we have focused on static¹⁶ bulk geometries and indicated how to extract certain details about the geometry from the boundary correlators. In this section we finally apply the relation between null geodesics and singularities of boundary correlators to the fully dynamical case of gravitational collapse. Previous studies of black hole collapse in the AdS/CFT context are [17-20].

The basic question we want to ask is: Can we see horizon formation directly in the gauge theory? Since in the bulk, horizon formation is a sharply-localized event (despite the fact

¹⁵At some special values of r and t , it is possible for them to coincide.

¹⁶Although the eternal black hole spacetime is not globally static, the method sketched above only probed the static part of the geometry. We comment on extracting the details of the dynamical spacetime inside the horizon in Appendix C.

that we need to know the full future evolution of the spacetime to actually find the horizon), we would expect that there will correspondingly be some sharp feature in the gauge theory. We will start by considering the simplest toy model, which is that of a collapsing spherical null shell. However, our main result should be applicable to general gravitational collapse, as will be clear below.

5.1 Null geodesics in a gravitational collapse

Consider a null spherical shell in d -dimensional asymptotically AdS spacetime. We can take the metric inside and in the past of the shell to be pure AdS, and the metric outside and to the future of the shell to be Schwarzschild-AdS. The metrics for the interior and the exterior of the shell can be written as

$$ds^2 = f_{\text{in,out}}(r) dt_{\text{in,out}}^2 + \frac{dr^2}{f_{\text{in,out}}(r)} + r^2 d\Omega_{d-2}^2 \quad (5.1)$$

where

$$f_{\text{in}}(r) = r^2 + 1 \quad (5.2)$$

$$f_{\text{out}}(r) = r^2 + 1 - \frac{r_+^2}{r^{d-3}} \quad (5.3)$$

The mass of the black hole is proportional to r_+^{d-3} . As in the previous section, we will use r_+ to denote the horizon radius and the surface gravity of the black hole is given by

$$\kappa = \frac{2}{r_+} = \frac{1}{2} \frac{df_{\text{out}}}{dr} \Big|_{r=r_+} \quad (5.4)$$

with $\frac{1}{2\kappa}$ the inverse Hawking temperature. Note that the t coordinate jumps across the shell with the jump approaching zero at the boundary. In contrast, the r coordinate is physical (since it measures the proper area of the spheres in a spherically symmetric spacetime) and therefore varies continuously across the shell.

The Penrose diagram for the collapse is sketched in Fig.8. There is only one asymptotic region; below the shell, the spacetime is pure AdS, whereas above, it is exactly Schwarzschild-AdS.¹⁷ The two important times, which are labeled in Fig.8 (a), are the time of the creation of the shell, t_s , and the time of the horizon formation. In global coordinates, the latter occurs in the bulk at the origin $r = 0$ at $t = t_h$; however, this need not correspond directly to the CFT time, since we're describing an event at $r = 0$ rather than at $r = 1$. Instead, the important CFT time related to the horizon formation is given by $t = t_h$ (labeled on the

¹⁷The singularity is drawn with a tilt for more realistic representation of the Penrose diagram in $d > 3$ dimensions (the shape of the singularity depends on d and r_+); however, here the "Penrose diagram" is to be treated as a sketch for ease of visualisation rather than an exact causal diagram.

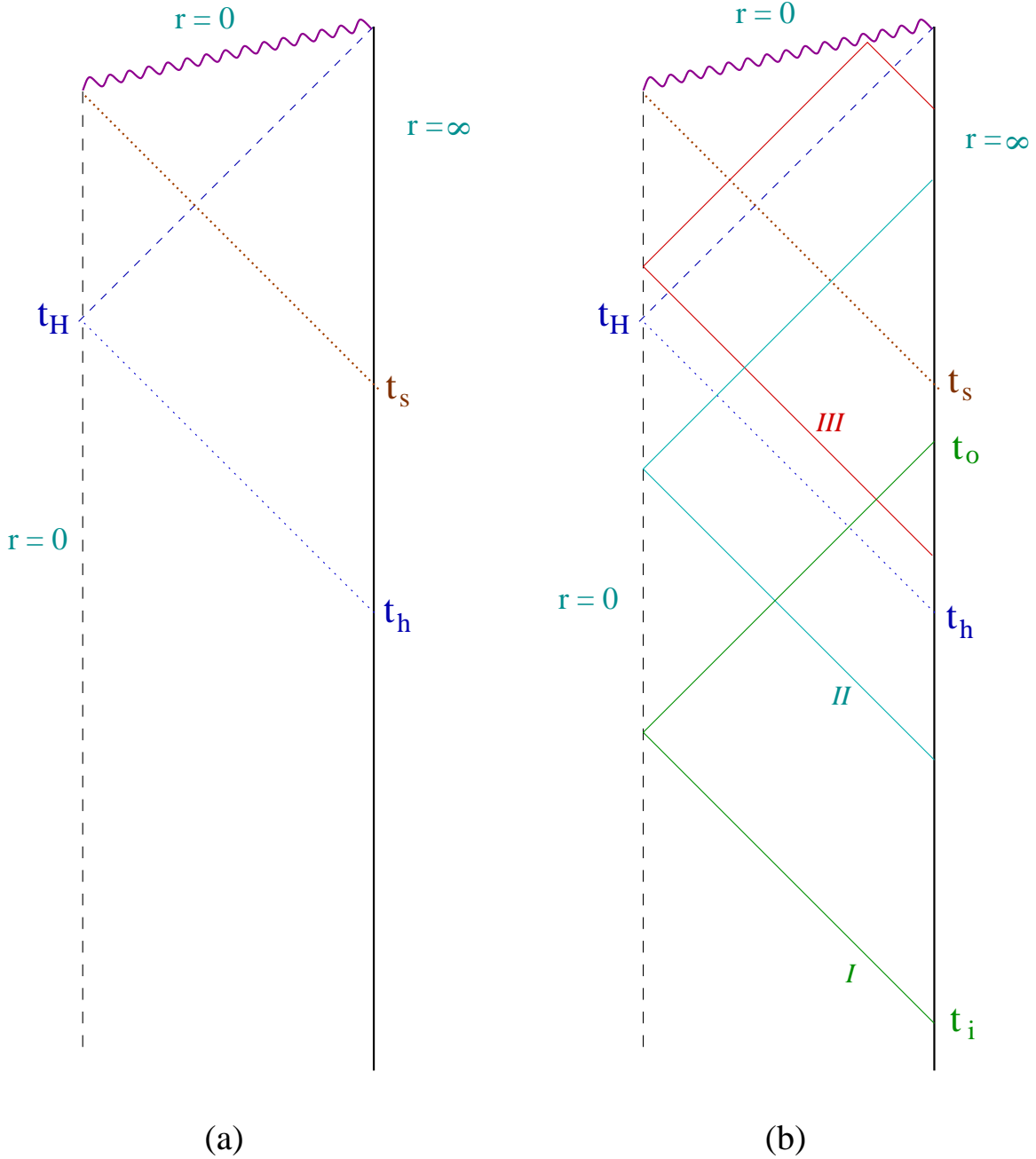


Fig. 8: Penrose diagram for a collapsed black hole. (a) shows the times for the shell creation and horizon formation; (b) in addition illustrates three distinct regimes of radial null geodesics. (Note that the last (upper right) part of geodesic III is only relevant for nearly-null spacelike geodesics which can bounce off the singularity. Also, to avoid cluttering the diagram, the starting time t_i and ending time t_o are labeled only for geodesic I.)

boundary), which is the time from which a radial null geodesic would have to start in order to hit the horizon formation event ($r = 0; t = t_H$).

Since this is a time-dependent geometry, the behavior of a null geodesic depends on the time t_i of the initial point. Radial null geodesics therefore separate into three qualitatively distinct classes, indicated in Fig.8 (b):

- I. For $t_i < t_s$, the geodesic is given by that of the pure AdS, and $t_0 < t_s$.
- II. For $t_s < t_i < t_h$, the geodesic starts out in AdS, crosses the shell at some point outside the horizon, and continues in Schwarzschild-AdS, reemerging to the boundary at $t_0 > t_s$.
- III. For $t_h < t_i < t_s$, the geodesic starts out in AdS but crosses the shell at some point inside the horizon, and therefore hits the singularity (the last part of the geodesic III sketched in Fig.8 (b) pertains to nearly null spacelike geodesics which can bounce off the singularity). For $t_i > t_s$, the radial null geodesic starts out in Schwarzschild-AdS and therefore crashes into the singularity; whereas for the nearly-null spacelike geodesics, this case is already covered above by reversing the orientation.

We discussed geodesics in AdS and Schwarzschild-AdS spacetimes in previous sections; here we match them together to analyse the behaviour in the collapse geometry. We focus on null geodesics of Type B, with $t_i > t_s$; this will be the interesting regime where we can probe the event horizon formation. Note that $t_h > t_s$, with t_h occurring earlier for larger black hole. In particular, using ray tracing within the AdS spacetime one can show that the horizon formation time is related to the shell creation time t_s and its mass, or equivalently r_+ , by (see Appendix E for a derivation)

$$t_h = t_s + 2 \tan^{-1} r_+ : \quad (5.5)$$

Let us first consider radial null geodesics. From the Penrose diagram, it is clear that as $t_i \rightarrow t_h$ from below, $t_0 \rightarrow \infty$, while for $t_i > t_h$, the null geodesic falls into the singularity and does not come back to the boundary. Since this will constitute the sharp CFT signature of the horizon formation event in the bulk, let us examine this feature in greater detail. The manner in which t_0 diverges as $t_i \rightarrow t_h^-$ can be obtained by following Hawking's ray tracing argument [21], which gives

$$t_0 = \frac{1}{\kappa} \log t + \text{constant} \Rightarrow t = e^{\kappa t_0} \quad (5.6)$$

where κ is the surface gravity of the black hole.¹⁸ To see (5.6), consider a point P_+ on the horizon just outside the shell. Let v to be the vector tangent to the horizon at P_+ and u

¹⁸Intuitively Eq.(5.6) reflects the fact that the redshift experienced by the outgoing null ray increases exponentially with t_0 as $e^{\kappa t_0}$ when $t_0 \rightarrow \infty$.

be the null vector directed normally outward from the horizon normalized so that $u \cdot v = 1$. The vector at P_+ which connects the horizon with the null geodesic can thus be written as u for some e . As $t_0 \rightarrow 1$, e can be expressed in terms of t_0 as

$$A e^{t_0}; \quad t_0 \rightarrow 1 \quad (5.7)$$

with A some constant independent of t_0 . Now parallel transport u and v across the shell to the point P on the horizon just inside the shell.¹⁹ remains invariant under this transformation. At P one can express e in terms of t as

$$B t \quad (5.8)$$

with some constant B . Comparing (5.7) and (5.8), we obtain the desired relation (5.6).

Note that the leading behavior (i.e., the logarithmic dependence) in (5.6) is rather robust, independent of the collapsing configuration and the type of black hole formed (charged, rotating). In Appendix E we also give alternative derivation of (5.6) for some explicit examples. While our arguments so far were of a qualitative nature, we can make rather precise predictions for where the singularity in the collapse state correlators should appear. This is carried out in some detail in Appendix E, where we calculate t_0 in terms of t_i and the parameters describing the state, t_s , r_+ , and α , to be

$$t_0 = t_s + \frac{2}{r_+} (1 + r_+^2) \frac{1}{2} (1 + \alpha^2) \tan^{-1} \frac{r_c}{1 + r_+^2} + r_+ \tanh^{-1} \frac{r_c}{r_+} \quad (5.9)$$

where r_c denotes the crossing radius where the geodesic intersects the shell, $r_c = \tan \frac{t_s - t_i}{2}$.

To summarize, we find that radial null geodesics are sensitive probes of horizon formation. The infinite redshift at the horizon translates into a sharp time scale t_h (5.5) at the boundary.

Now let us consider non-radial null geodesics. A natural question is whether there exists an analogous value $t_h(\alpha)$ for each $\alpha = E = J$ so that as $t_i \rightarrow t_h(\alpha)$, the corresponding $t_0 \rightarrow 1$. The answer turns out to be yes for a range of values of α , but for a different reason from that for the radial geodesics. By the very nature of an event horizon, we expect that the only null geodesic which truly samples the event horizon formation is the radial one; any other null geodesic which approaches the horizon non-radially cannot escape to the boundary. In Appendix F, we describe how to compute $t_h(\alpha)$ for general α . We show that all geodesics with angular momentum for which t_0 diverges take that long to reach the boundary not because of being trapped near the event horizon, but rather because of circling around a null circular orbit at a given finite distance outside the horizon.

It is easy to see that $t_h(\alpha)$ depends non-trivially on α ; the presence of angular momentum causes the geodesic to sample a different region of the spacetime geometry. In the limit

¹⁹Note that u and v are continuous when crossing the shell.

²⁰Since the shell geometry is not static, E jumps across the shell; in defining t_h we use the initial E i.e., its value in pure AdS.

! 1 (maximal angular momentum) we expect that the geodesic stays arbitrarily close to the boundary, so that it doesn't sample the black hole geometry, and in particular there can be no divergence in t_c for any finite t_i . In the opposite limit of zero angular momentum, we have already seen that $t_h(1)$ is given by the expression for t_h for the radial geodesic (5.5). The result of Appendix F is summarized in Fig. 9, which plots $t_h(\alpha)$ as a function of $J = 1 - \alpha$. In particular, we note that:

$$\begin{aligned} t_h(\alpha) & \rightarrow t_h = t_s - 2 \tan^{-1}(r_+) ; & \alpha & \rightarrow 1 \\ t_h(\alpha) & \rightarrow t_s ; & \alpha & \rightarrow 0 \end{aligned} \tag{5.10}$$

while for $1 < \alpha < \alpha_0$, t_c never diverges, where α_0 was introduced in (4.6). Recall that the Schwarzschild-AdS geometry contains a null circular orbit with $\alpha = \alpha_0$ at $r = \sqrt{\frac{2}{3}}$. As Fig. 9 demonstrates, $t_h(\alpha)$ is not a monotonic function of $1 - \alpha$. In particular, the minimal value of $t_h(\alpha)$, which we will denote as t_c , is smaller than t_h , the horizon formation time. t_c is the boundary time scale at which the null circular orbit of the newly formed black hole geometry is first probed.

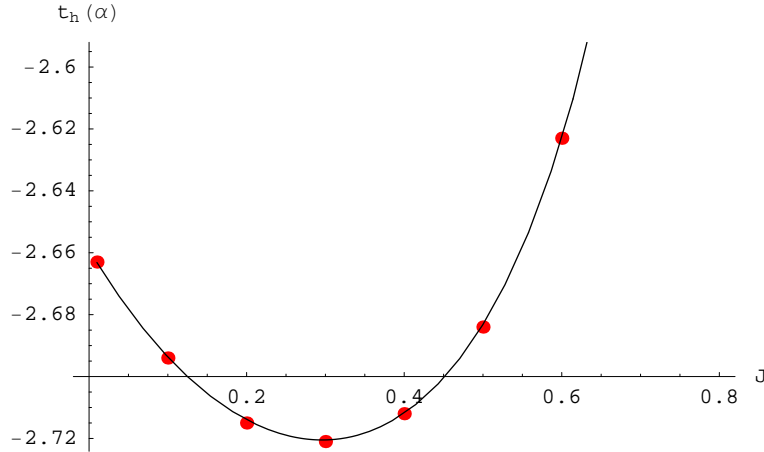


Fig. 9: Variation of $t_h(\alpha = \frac{1}{J})$ as a function of angular momentum J in the thin shell spacetime (5.1) (solid line). The intersection of the curve with vertical axis gives t_h , while the minimum gives t_c . Red dots are data extracted from Fig.11, which were obtained by numerical integration of the geodesics in the Vaidya spacetime (5.12), (5.13) with $v_s = 0.001$.

In Fig.10, we plot the endpoints of various geodesics on the $t - \theta'$ plane²¹ for a fixed initial time $t_i \geq (t_s - t_c)$. Note that in contrast to the analogous plots in earlier sections for other geometries, the background here does not have a time translational symmetry. For ease of visualization we unwrap the θ' direction and at the same time compactify both the

²¹Since θ' is the only continuous free parameter describing the null geodesics, this will produce a curve of endpoints on the $t - \theta'$ plane.

t and ϕ so that we can examine the full $(\phi; t)$ plane. For each fixed t_i , we plot the end-point curve, color-coded by ϕ . For $t_i < t_c$, the endpoints would all clump into the single point $(\phi; t) = (0; 0)$. As we increase t_i so that the geodesics start sampling the shell, the endpoints begin to spread in the manner shown on the left in Fig.10, into a cusp similar to the star geometry (cf. Fig.5). As t_i reaches the minimum of the curve $t_h(\phi)$ shown in Fig.9 (i.e., $t_i = t_c$), the cusp extends to $(\phi; t) = (1; 1)$ (upper right corner of the plots) with

$$t(\phi) = \frac{1}{\tan^2 \phi} \quad (5.11)$$

Increasing t_i further, the cusp still reaches $(\phi; t) = (1; 1)$ with (5.11), but now for two different values of ϕ , given by solution to $t_h(\phi) = t_i$. At the same time, t for the radial geodesic increases, diverging as $t_i \rightarrow t_h$. This will appear in Fig.10 as the left end point of the upper branch moving to $(0; 1)$. The right plot in Fig.10 is taken for t_i slightly smaller than t_h . Note that equation (5.11) follows from the fact that as $t_i \rightarrow t_h(\phi)$, the geodesic goes around the circular null orbit with a period $\frac{2}{\omega_0}$ in ϕ many times.

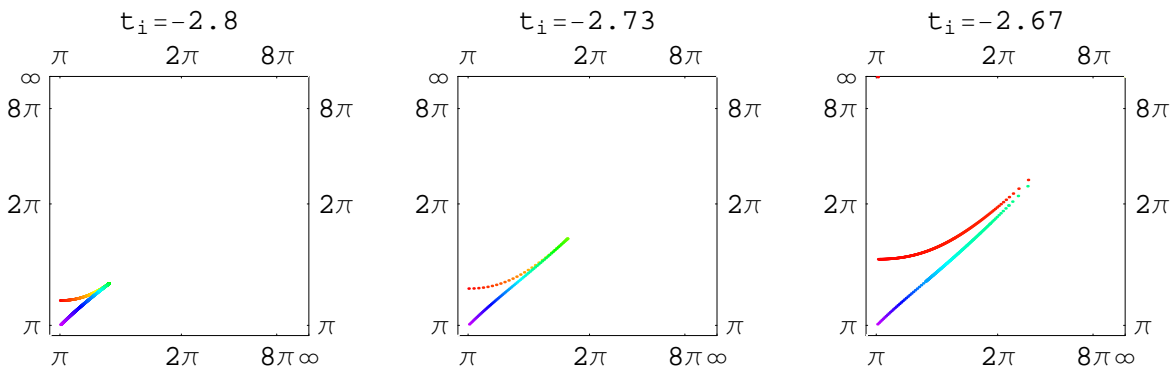


Fig. 10: Plot of $(\phi; t)$ for 3 values of t_i in the thin shell geometry (same configuration as in Fig.9 and Fig.11 (a)), for various values of ω_0 (1;1). The horizontal and vertical axes show ϕ and t respectively, rescaled by $\tan^2 \phi$ to fit the full plane. The left endpoint of the upper branch corresponds to $\phi = 1$ (radial geodesic), while the left endpoint of the lower branch corresponds to $\phi = 0$. (a) $t_i = -2.8 < t_c = -2.72$; (b) $t_i = -2.73$ only slightly smaller than t_c ; (c) $t_i = -2.67$ slightly smaller than $t_h = -2.66$. Here t_c is the minimal value of the curve in Fig.9 and t_h is intersection of the curve in Fig.9 with the vertical axis. As $t_i \rightarrow t_c$ the cusp should reach $(1; 1)$ (upper right corner) and as $t_i \rightarrow t_h$, the left endpoint of the upper branch should reach $(0; 1)$ (the upper left corner). Note that as apparent from Fig.11, the endpoints vary rather sharply with t_i for $t_i \rightarrow t_h(\phi)$, so it is difficult numerically to sample the large values of ϕ, t .

One can generalize the sharp shell to a smeared-out version which is physically more

realistic. To that end, we consider a Vaidya spacetime of the form

$$ds^2 = -f(r;v) dv^2 + 2 dv dr + r^2 d\Omega^2 \quad (5.12)$$

with $f(r;v)$ smoothly transitioning between (5.2) at $v \rightarrow -1$ and (5.3) as $v \rightarrow +1$; a convenient form to use is

$$f(r;v) = r^2 + 1 - \frac{1 + \tanh \frac{v}{v_s}}{2} \quad (5.13)$$

In particular, the shell is inserted at $v = 0 = t_s + 2$, and has 'thickness' v_s . As $v_s \rightarrow 0$, we recover the collapse spacetime (5.1) written in ingoing coordinates.

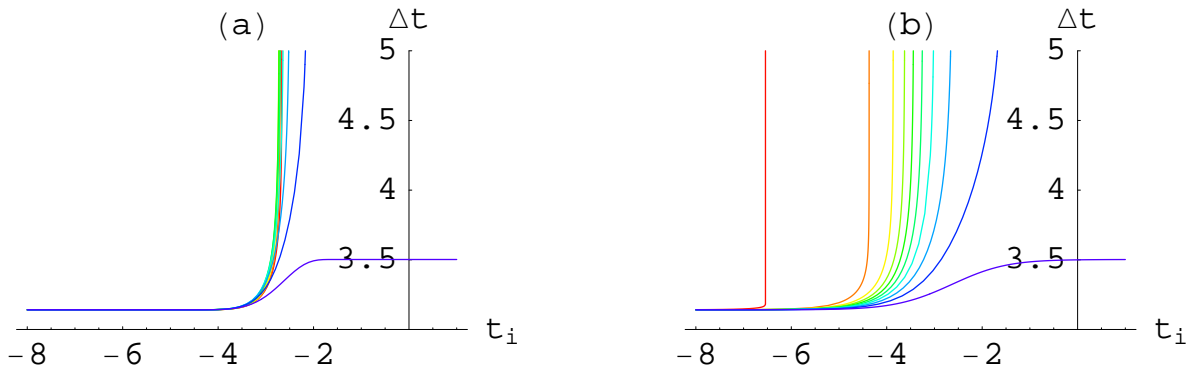


Fig. 11: Plot of Δt as a function of t_i for non-radial null geodesics in the Vaidya metric with the effective "thickness" of the shell given by (a) $v_s = 0.001$ and (b) $v_s = 1$. The various curves differ in angular momenta, $J = 0.01; 0.1; 0.2; 0.3; \dots$.

Fig.11 shows the value of $t = t_0 - t_i$ for a set of non-radial geodesics in the spacetime (5.12) with various values of J , all starting at the initial time t_i ; in (a) the shell is very thin whereas in (b) the shell is considerably smeared out. The value of $t_h(J)$ can be read off from the plot; it corresponds to the value of t_i at which Δt diverges for a geodesic with that J . For the thick shell in Fig.11 (b), we see that these times are well-separated, and increase monotonically with increasing $J=E$ (decreasing ℓ).

This illustrates that the sharp signature of the horizon formation event is not limited to the thin-shell collapse (bulk spacetimes with a null shell sharply separating pure AdS from Schwarzschild-AdS): For any spherically symmetric spacetime in which an event horizon forms at a time t_h at the origin, reachable by an ingoing radial null geodesic starting at the boundary at t_h , we can find t_h by exactly the same method. In particular, our method constitutes following the red (leftmost) curve in Fig.11 (b).

To summarize, whereas only the radial null geodesic starting at t_h samples the horizon formation event, the non-radial null geodesics provide further details about the geometry, in

particular the null circular orbit of the newly formed black hole geometry. Furthermore the variation of the curves $t(\rho)$ with respect to t_i provides spatio-temporal information both dynamically around the horizon formation time and spatially in the vicinity of the horizon.

5.2 Gauge theory signatures

We can now translate the behaviour of null geodesics in the bulk collapse spacetime to predictions regarding boundary correlation functions. Our discussion below should apply to generic highly excited states in the boundary theory²².

Consider the CFT correlators of the form $\langle hO(t_i; \rho)O(t_o; \rho) \rangle_{i_{\text{shell}}}$ evaluated explicitly in the state of the shell. Modelling the shell as being created by an operator S inserted in the boundary at $t = t_s$, we have

$$\begin{aligned} \langle hO(t_o; \rho)O(t_i; \rho) \rangle_{i_{\text{shell}}} &= \langle hO(t_o; \rho)O(t_i; \rho) \rangle_{\text{AdS}}; & t_i < t_o < t_s \\ &= \langle hO(t_o; \rho)O(t_i; \rho)S(t_s) \rangle_{\text{AdS}}; & t_i < t_s < t_o \\ &= \langle hO(t_s; \rho)O(t_o; \rho)O(t_i; \rho)S(t_s) \rangle_{\text{AdS}}; & t_s < t_i < t_o \end{aligned} \quad (5.14)$$

By our previous arguments, we would expect this correlator to become singular when the insertion points are connected by a null geodesic. More explicitly,

- I. When $t_o < t_s$, the correlator is simply the standard vacuum two point function. The singularities are given by the usual light cone singularities of the boundary theory. As is clear from geodesic I in Fig.8 (b)), all null geodesics lie entirely in the AdS region.
- II. When $t_i < t_s < t_o$, the correlator is given by the second line of (5.14). From our discussion of null geodesics in last subsection, the pattern of bulk-cone singularities for this correlator has a rich structure, which reflects the formation of the event horizon and the null circular orbit in the bulk.

Suppose experimentalists in the boundary theory are able to measure the observable $\langle hO(t_i; \rho)O(t_o; \rho) \rangle_{i_{\text{shell}}}$ for all t_i and t_o satisfying $t_i < t_s < t_o$. Then by carefully plotting the locations of singularities of the correlator in the $t-\rho$ plane for a given t_i , they should recover various plots of Fig.10. In particular two distinct time scales emerge by comparing the pattern of singularities for different t_i . The first is the time t_c when the cusp in Fig.10 reaches $(1; 1)$. This is the time scale that non-radial null geodesics originating from the pure AdS geometry start being trapped by the circular orbit of the newly formed black hole. The slope of the line reaching the infinity gives the period of the orbit. The second is the time t_h that the left end of the upper branch

²²By highly excited states we mean states of energies of order dN^2 , with N -independent constant c sufficiently big. By generic states we mean states which are generic superpositions of energy eigenstates. Note that energy eigenstates do not give rise to the desired time dependence.

(which corresponds to radial geodesics) reaches $(\frac{1}{2}; 1)$. This is the time of horizon formation as probed by a radial null geodesic. The bulk time of horizon formation in global AdS coordinates is given by $t_H = t_h + \frac{1}{2}$.

III. When $t_s < t_i < t_o$, the correlator is given by the third line of (5.14). In this case, all singularities of the correlator are the same²³ as those of a finite temperature correlation function with the temperature T given by

$$\frac{1}{T} = \frac{\partial \log \rho(E)}{\partial E} \quad (5.15)$$

where E is the energy of the shell state and $\rho(E)$ is the density of states of the CFT. This follows from that all type B geodesics with $t_s < t_i < t_o$ are identical to those of an AdS black hole.

In the above we discussed the pattern of bulk-cone singularities of (5.14). There might also be more subtle signals, on a secondary sheet (so we would find the singularity in the correlator only after a suitable analytic continuation) when the insertions are separated by a spacelike geodesic which is arbitrarily close to being null as illustrated for the eternal black hole singularity in [6]. In other words, the corresponding geodesic passes through the black hole and bounces off the singularity²⁴, see e.g. geodesic III of Fig.8 (b). Such a situation could arise when $t_i > t_h$ (which, if we define $t_i < t_o$, also implies that $t_i < t_s < t_o$). We will discuss it in more detail in Section 5.3.

5.3 Signature of the black hole singularity?

In addition to the null geodesics considered in Fig.8, it is also of interest to consider some spacelike geodesics. In particular, spacelike geodesics have the important feature that they bounce off the black hole singularity [6], and thus could provide valuable information about the black hole singularity. There are two other types spacelike geodesics in the collapse background which are of particular interest (see Fig.12):

1. $t_i > t_h$ from above and $t_o > 1$. As can be seen from Fig.12a, the geodesic passes inside the horizon and bounces off the singularity. We will calculate below the dependence of t_o on $t = t_h - t_i$.
2. As $t_i > t_s, t_o > t_s$: The corresponding geodesic is sketched in Fig.12b. One expects that $t_o = t_s + \delta(t_h - t_i)$, where δ should depend on how strongly geodesics are repelled from the singularity.

²³The correlator itself does not necessarily coincide with a thermal correlation function. Only the singularity structure does.

²⁴However, note that there is no longer a single radial null geodesic connecting the insertion points.

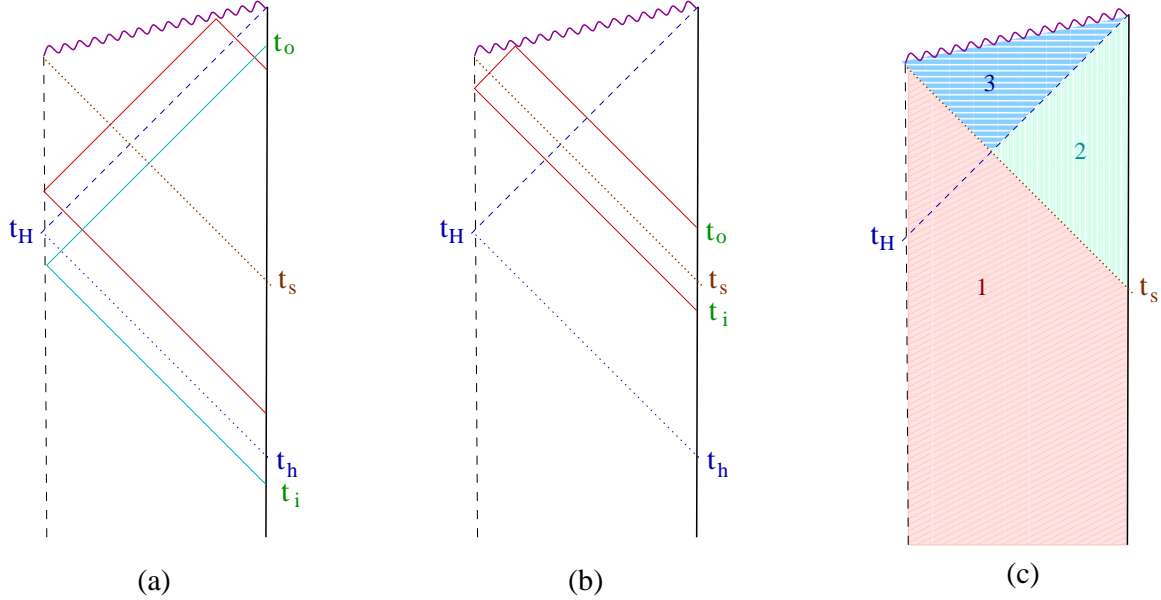


Fig. 12: Penrose diagram for a collapsed black hole

Note that spacelike geodesics are parameterized by E and J , but here we set $J = 0$ to focus on radial geodesics, and moreover we take the infinite E limit, so that their trajectories converge to the radial null geodesics, except for the important point that they bounce off the black hole singularity. As before, we can find geodesics in the full collapsing geometry by patching the geodesic segments in the respective regions; here in addition to AdS (region 1 in Fig.12c) and the Schwarzschild-AdS region outside the horizon (region 2 in Fig.12c), we now have to consider Schwarzschild-AdS inside the horizon as well (region 3 in Fig.12c). This is presented in detail in Appendix E; here we only quote the main results.

1. As $t_i \rightarrow t_h^+, t_o \rightarrow 1$ in the same manner as for $t_i \rightarrow t_h$ (cf. Eq.(5.6)), namely:

$$t = t_h - t_h e^{-t_o} \quad (5.16)$$

2. Let $t_s = t_h + \epsilon$. Then expanding $t_h - t_h$ to third order in ϵ , we find that

$$t_o = t_h + \epsilon^{\frac{d-2}{2}} : \quad (5.17)$$

with a coefficient which depends on the parameters of the final black hole (see (E.16)).

As argued around (5.6), it is clear that the behaviour (5.16) is robust and is expected to hold in any spacetime dimension. The behaviour of the geodesic which bounces off the singularity in Fig.12b, and in particular the exponent $\frac{d-2}{2}$, depends crucially on the dimension; $\frac{d-2}{2} = d - 2$ in AdS₃. Intuitively this is due to the fact that the curvature of the singularity increases with spacetime dimension.

6 Discussion

We have argued that the AdS/CFT correspondence implies the existence of "bulk-cone singularities" in boundary theory correlation functions, which lie inside the light-cone. The pattern of singularities can in turn be exploited to extract information about the bulk geometry. Our argument revolved around the essential point that Green's functions for quantum fields in curved space are singular when the arguments are null separated. While the geodesic approximation was necessary to derive the conclusion, we should point out that one expects the result to be true as long as it makes sense to talk about the spacetime geometry. In other words, we expect validity in \hbar^0 expansion, but not necessarily in g_s expansion (where it is plausible to have a breakdown of the geometric picture).

We have demonstrated the pattern of singularities in the field theory correlators for several distinct scenarios: in radiation star, eternal Schwarzschild-AdS black hole, and the geometry of a collapsing shell. We have seen that small deformations of bulk geometries can in principle produce significant differences in the structure of singularities which are discernible on the boundary. In this context it is also satisfying that the vacuum state of the CFT, corresponding to pure AdS spacetime, has a distinguished role, as evidenced by the theorem of [3]. Further, we are guaranteed that bulk-cone singularities for correlators evaluated in excited states occur at later times compared to the vacuum correlators, as necessitated by causality.

The novel application of our proposal was to the case of dynamical spacetimes. We concentrated on the simple scenario of a null shell collapse in AdS/CFT. One of the fascinating aspects of the singularity structure of the correlations is that they encode the spacetime event corresponding to event horizon formation in the bulk unambiguously. The characteristic signature we discussed is quite robust and can be easily distinguished from other singularities in the correlation functions. Further, the detailed pattern of singularities carries information about the geometry of the black hole that is formed. By using the non-local nature of the correlation functions we are able to extract information about the details of the bulk spacetime, while, in contrast to the recent discussions of probing the black singularity in AdS/CFT [6, 7], we are not reliant on analytic properties of the CFT correlators.

It would be very desirable to test our predictions of the existence of the bulk-cone singularities directly within the boundary theory. Note that the classical limit corresponds to the large N and large 't Hooft coupling limits of the boundary theory. It would be interesting to understand whether the appearance of bulk-cone singularities for correlation functions in excited states is an artifact of the large N and/or large 't Hooft coupling limits, or a generic feature for field theories on compact spaces.²⁵

An intriguing avenue to explore is to extend these considerations to microstate geom-

²⁵Note that bulk-cone singularities do not arise for non-compact boundary as shown in Appendix D.

tries" proposed for black hole spacetimes. In situations where we have an explicit map between the spacetime geometries and the field theory states such as two charge D1-D5 system [15,16], the 1/2 BPS sector of $N = 4$ SYM [14], one can ask whether the pattern of singularities differs significantly between different states. The general arguments regarding the correlation functions of typical states that comprise the black hole entropy in [22,25] would seem to suggest that the structure of the singularities is not capable of discerning the fine distinctions between the geometries. This is however counter to the gravitational intuition: naively one expects geometries that differ from each other to have differing behaviour of Green's functions, especially with regard to the location of the singularities. A potential resolution of this discrepancy is that the geometric picture is incorrect for the "microstate geometries" as one has to consider a suitable wavefunction over the quantum moduli space of solutions. This is an interesting question that deserves to be explored further.

Another interesting generalization of our set-up would be to model the AdS/CFT analog of Choquetuk scaling [26]. Given that we have a specific prediction for the field theory signature of black hole event horizon formation, one can ask whether the critical behaviour observed during the collapse has a field theoretic image and map out the details of the correspondence in this case.

Acknowledgements

We would like to thank Allan Adams, Dan Freedman, Gary Horowitz, Bob Jaeger, Albion Lawrence, Don Marolf, Simon Ross, Steve Shenker, Amit Sever for discussions. We would also like to thank KITP, Santa Barbara for kind hospitality during the "Scanning New Horizons: GR beyond 4 dimensions" program where this project was initiated. VH and MR would also like to thank the Aspen Centre for Physics for hospitality during the concluding stages of this project. HL is supported in part by the A.P. Sloan Foundation, the U.S. Department of Energy (DOE) OJI program and by the DOE under cooperative research agreement # DF-FC02-94ER40818.

Appendix A : Pure AdS

For ease of comparison of our results on the star and other geometries in what follows, we first summarise the basic facts regarding geodesics in AdS, concentrating on null and spacelike geodesics.

A.1 Geodesics in AdS: summary

Consider $d+1$ -dimensional AdS in global coordinates. The metric can be written as

$$ds^2 = -f(r) dt^2 + \frac{dr^2}{f(r)} + r^2 d\Omega_{d-1}^2 \quad (\text{A.1})$$

$$f(r) = 1 - r^2 :$$

The geodesic equations are as in (4.4), with $f(r)$ being that given in (A.1).

As we are primarily interested in the endpoints of null or spacelike geodesics (ultimately with diverging regularised proper length). To that end, the useful quantities are the temporal and angular separation of the geodesic endpoints, which we denote by t and θ' , respectively. Let us first focus on spacelike geodesics, since as we will see, these limit to null geodesics. We can integrate the geodesic equations to obtain:

$$t = \frac{L}{2} + \sin^{-1} \frac{E^2 - J^2 - 1}{e^L} \quad (\text{A.2})$$

$$\theta' = \frac{L}{2} + \sin^{-1} \frac{E^2 - J^2 + 1}{e^L} \quad (\text{A.3})$$

$$e^L = \frac{P}{(E^2 - J^2)^2 + 2(E^2 + J^2) + 1} \quad (\text{A.4})$$

where L is the geodesic length after regularising away the divergent piece $\log R_C^2$ (R_C is the radial cut-off). Finally, another useful expression is the minimum r value reached by the geodesic r_{min}

$$2r_{\text{min}}^2 = (E^2 - J^2 + 1) + e^L \quad (\text{A.5})$$

From the expression for e^L it is clear that we have a large negative length when

$$1. E \gg 1 \text{ with } J \text{ fixed} \Rightarrow L \approx \log E^2$$

$$2. J \gg 1 \text{ with } E \text{ fixed} \Rightarrow L \approx \log J^2$$

$$3. J \approx E \gg 1 \Rightarrow L \approx \log E$$

Now consider two boundary points A and B are separated by boundary coordinate distance $t = t_A - t_B$ and $\theta' = \theta'_A - \theta'_B$. We can easily see that for any spacelike separation $0 < t, \theta' < \pi$, there is a unique geodesic joining A and B; specially we can calculate E and J for the geodesic given t, θ' :

$$E = \frac{\sin \theta'}{\cos \theta' - \cos t} \quad (\text{A.6})$$

$$J = \frac{\sin t}{\cos \theta' - \cos t} \quad (\text{A.7})$$

and its length is

$$L = -\log 2 + \log(\cos \theta' - \cos t) \quad (\text{A.8})$$

A.2 Spacelike vs. null geodesics

Null geodesics in AdS only connect points with $t = \tau = \phi$, irrespective of the parameter $E = J$. While this is a well known fact for radial null geodesics (for which $J = 0$), it is true that even geodesics carrying angular momentum emerge at the anti-podal point on the sphere in exactly AdS time. As mentioned in Section 2 these null geodesics endpoints being coincident with the endpoints of purely boundary null geodesics, we do not see extra singularities in the correlation functions.

A naive puzzle about the null limit arises when we consider the difference between the angular separation of the endpoints ϕ for spacelike and null geodesics. Spacelike geodesics in AdS allow any $0 < \phi < \pi$; indeed for $E = 0$ (constant t slice) the geodesics plotted on the Poincare disk are circular arcs with diameter related to the angular momentum. On the other hand, null geodesics always reemerge at the anti-podal point $\phi = \pi$. How do the geodesics change their behaviour as we take $E \rightarrow 1$ at fixed J ? Fig. 13 illustrates this limit.

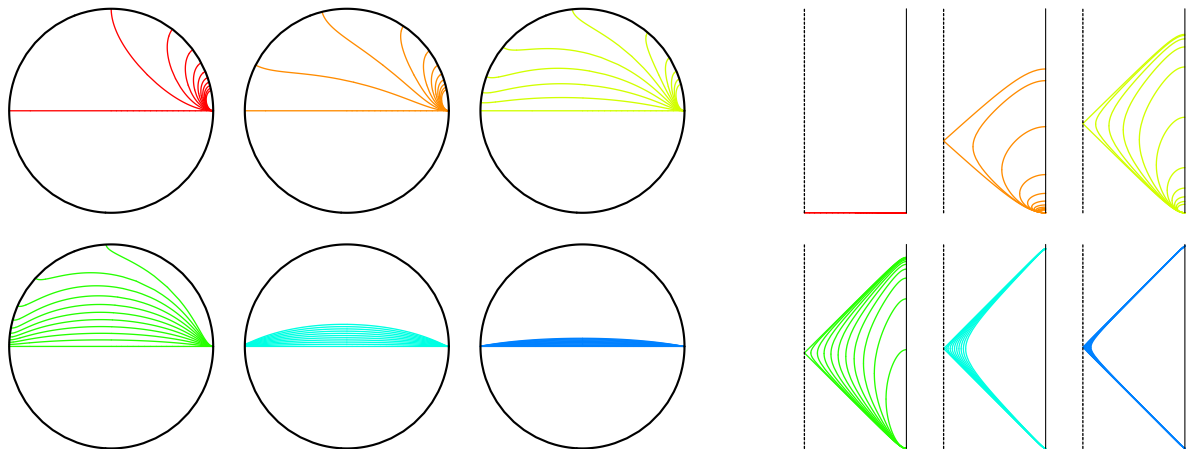


Fig. 13: Spacelike geodesics in AdS, projected to a constant t slice (left) and the $t-r$ plane (right), for six different values of energy ($E = 0; 2; 5; 10; 30; 80$). For each E , geodesics with different values of angular momentum ($J = 0; 1; 2; \dots; 10$) are plotted. The bold circles represent the boundary at $\tan r = \frac{\pi}{2}$. The dashed vertical lines correspond to the origin $r = 0$ and the bold vertical lines to the boundary at $\tan r = \frac{\pi}{2}$. The range of t plotted is $(0; \infty)$.

For any fixed finite J , as $E \rightarrow 1$, we see that the geodesic indeed converges to the radial null geodesic and $\phi \rightarrow \pi$.

Nevertheless, the full set of singularities of the boundary correlation function (2.10) is larger than those captured by the points with $t = \tau = \phi$. It is interesting to ask whether there are any bulk geodesics (with divergent regularized proper length) that connect points with $t = \tau \notin \phi$. From (A.4), one concludes that the regularised proper length along a

spacelike geodesic diverges not only when $E \rightarrow 1$, but also when $J \rightarrow 1$. Does this mean that this is an equally good null limit, and that therefore $t = t'$? The answer is no: as we can see from (A.3), as $J \rightarrow 1$ at fixed E , $t' \rightarrow 0$. The geodesic has vanishing proper length because it is so short rather than because its tangent vector is null. On the boundary, this corresponds to the usual divergence of correlator of operators inserted at the same point.

However, it turns out that there nevertheless are nontrivial almost-null spacelike geodesics with $t = t' \neq 0$. Consider spacelike geodesics in AdS parameterized by E and J with the following constraint:

$$J^2 = E^2 - \epsilon \quad (A.9)$$

for some real number ϵ . Upon taking the limit $E \rightarrow 1$, we obtain

$$t \rightarrow \frac{1}{2} + \sin^{-1} \sqrt{\frac{\epsilon}{2 + 4\epsilon}} \quad (A.10)$$

$$t' \rightarrow \frac{1}{2} + \sin^{-1} \sqrt{\frac{\epsilon}{2 + 4\epsilon}} \quad (A.11)$$

Clearly, these are equal, and take the full range $0 < t = t' < \frac{1}{2}$ for $1 < \epsilon < 1$. Further, we can check that this family of geodesics indeed converge onto the boundary null geodesics. Fig.14 demonstrates these features. We see that as E increases, the geodesics

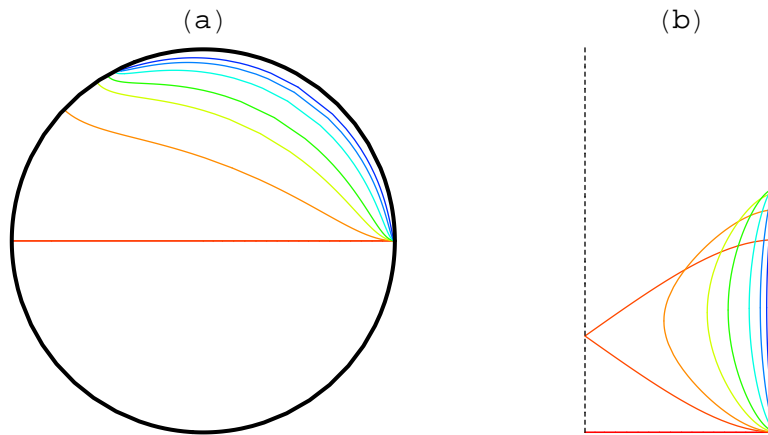


Fig. 14: Spacelike geodesics in AdS, projected to (a) a constant t slice and (b) the $t-r$ plane, for increasing values of energy and $J^2 = E^2 - \epsilon$ with $\epsilon = 1$ (in the infinite E limit this would yield $t = t' = \frac{1}{3}$). In (a) the boundary is indicated as the bold circle. In (b) the boundary at $\tan r = \frac{1}{2}$ is in bold and the dashed vertical line is the origin.

accumulate at a finite value of t and t' , in this case being $1, \frac{1}{2} + \sin^{-1} \sqrt{\frac{1}{5}} = \frac{1}{3}$.

To summarise this discussion, in pure AdS_{d+1} spacetime, null geodesics connect points on the boundary which are antipodally located on the S^{d-1} at a time separation $t = \frac{1}{2}$.

Spacelike bulk geodesics on the other hand connect points with $t = t_0$ as illustrated by (A.10) and (A.11), respectively (or more generally, (A.2) and (A.3)).

Appendix B: Radiation star in AdS

In this Appendix, we construct the geometry corresponding to a gas of radiation in AdS and study its properties. As sketched out in Section 3, constructing the solution entails specifying the form of the stress-energy-momentum tensor and solving the Einstein's equations.²⁶ After filling in the gaps in the presentation of Section 3, we extend our study of the star geometry by analysing spacelike geodesics, and then discuss the observable differences between the star geometry and that of a black hole.

B.1 Construction of the star-AdS spacetime

As discussed in Section 3, one can construct a simple model for a static, spherically symmetric, asymptotically AdS "star" geometry by solving Einstein's equations with a negative cosmological constant and matter given by a perfect fluid stress tensor corresponding to radiation. The metric coefficients are determined by solving the Einstein's equation

$$G_{ab} + \Lambda g_{ab} = 8\pi G_5 T_{ab} \quad (\text{B.1})$$

where for convenience we will set $8\pi G_5 = 1$ and $\Lambda = -6$ to set AdS radius to unity.

The symmetries constrain the metric to take the form (3.2). One can then infer the equations (3.3) and (3.5) from the tt component of the Einstein tensor. The rr component of the Einstein tensor yields

$$\frac{f'}{f} = \frac{2}{r} \frac{\frac{r^2}{R^2} + \frac{m(r)}{r^2} + \frac{1}{12} (r) r^2}{\frac{r^2}{R^2} + 1 - \frac{m(r)}{r^2}} \quad (\text{B.2})$$

which can be easily integrated to get $f(r)$ in terms of $m(r)$ and (r) . Finally, using the angular part of Einstein's equation, or equivalently the stress tensor conservation, we can write (for general equation of state)

$$\frac{dP}{dr} = -(P + \rho) \frac{1}{2} \frac{f'}{f} \quad (\text{B.3})$$

This can then be used to derive the system of coupled first order ODEs for $m(r)$ and (r) given by (3.6) and (3.7), respectively. The equation for $f(r)$, (B.2), can be simplified to (3.4) using the equations for $m(r)$ and (r) .

²⁶Analogous calculations in 4 dimensions were discussed in [27], with similar qualitative results as we obtain below.

B.2 Geodesics in the star geometry

In Section 3 we examined some aspects of the star geometry by focusing on null geodesics; here we extend this analysis to spacelike geodesics as well. While these do not lead to singularities of the boundary correlators, they nevertheless reveal interesting points. Since

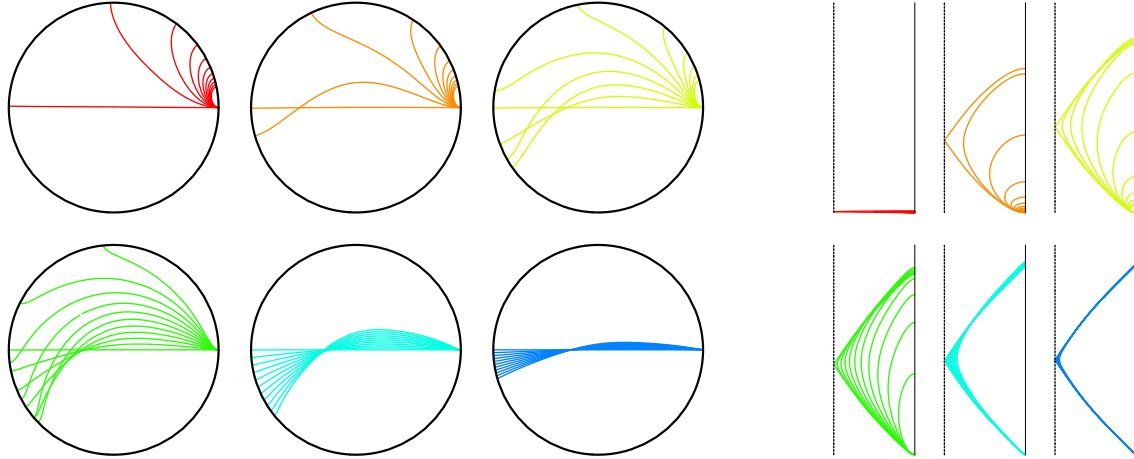


Fig. 15: Spacelike geodesics in star with $t_0 = 10$ in AdS, projected to a constant t slice (left) and the $t-r$ plane (right), for six different values of energy ($E = 0; 2; 5; 10; 30; 80$). For each E , geodesics with different values of angular momentum ($J = 0; 1; 2; \dots; 10$) are plotted. The bold circles represent the boundary at $\tan r = \frac{1}{2}$. The dashed vertical lines correspond to the origin $r = 0$ and the bold vertical lines to the boundary at $\tan r = \frac{1}{2}$. The range of t plotted is $(0; 1; 1 - t_0)$.

the star in AdS can be viewed as a deformation of the pure AdS geometry, it is particularly interesting to contrast the behaviour of spacelike geodesics in the star geometry with that in AdS. In Fig. 15 we show spacelike geodesics projected onto the constant t and $t-r$ plane (these plots are to be compared with Fig. 13, where same conventions apply). As for null geodesics, we see a focusing effect, created by the star in the center of AdS.

To see how the endpoints of these various geodesics compare, let us consider the values t and r for the various geodesics. Fig. 16 summarizes this. One interesting feature to note is that since the curves for various energies intersect each other, it is no longer true that for any two spacelike-separated points, there is a unique spacelike geodesic connecting them. In particular, unlike the pure AdS case, there is an open set of endpoints which can be reached by more than one geodesic. Even more remarkably, there exists a set of endpoints (lower branch of the thick pink curve in Fig. 16) which are connected by both a null and a spacelike geodesic! Also, as a corollary, it is no longer true that the endpoints of null geodesics lie on the boundary of the set of endpoints of spacelike geodesics. Correspondingly, the endpoints

of the null geodesics reflect this behaviour, as can be seen easily in Fig.5. While δ slowly increases with increasing ρ_0 , the endpoints never approach a straight line, as would be the case for the black hole geometry. This in turn means that the endpoints are less sensitive indicator of the star geometry than in the black hole case.

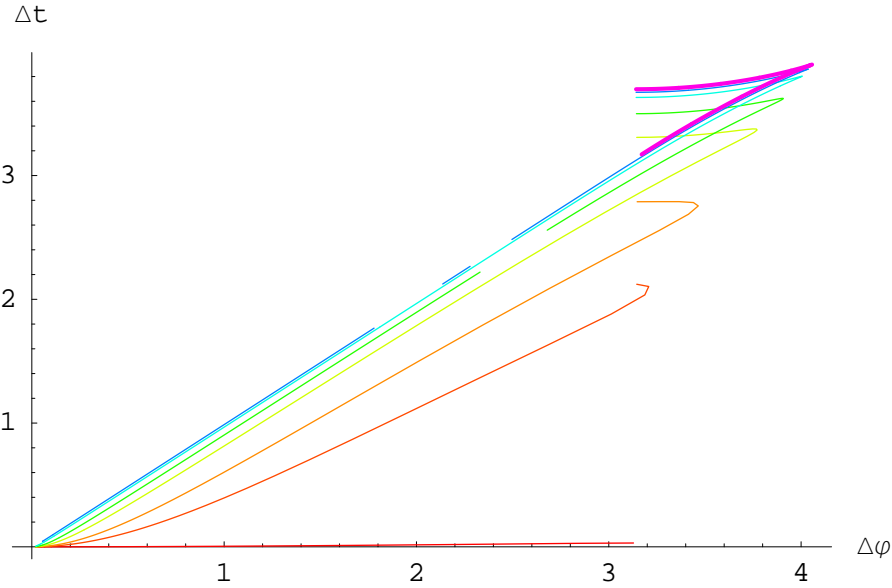


Fig. 16: Endpoints of spacelike and null geodesics in the geometry of star with $\rho_0 = 10$ in AdS. Spacelike geodesics for six different values of energy ($E = 0; 2; 5; 10; 30; 80$) and a null geodesic (thick pink curve) is plotted for varying values of J (varying J traces out curves in the $t-\phi$ plane; the top of the curves corresponds to small values of J , while in the large J limit, t and ϕ both approach their starting value, namely 0).

B.3 Comparison between star and black hole

Let us now ask how does the geometry vary with ρ_0 . Clearly, as $\rho_0 \rightarrow 0$, the geometry becomes that of pure AdS; hence the star's utility in studying small perturbations on AdS. One might naively expect that in the opposite limit, as we make the internal density very large, the star should start behaving more and more like a black hole. Unfortunately, this is not the case, as will be explained below.

First of all, to compare the star's geometry with that of a Schwarzschild-AdS black hole, the most sensible map of parameters is to identify the black hole's mass with the star's total mass, so that the asymptotic geometry matches. In other words, for the black hole, we use the metric of the form in (3.2), but with

$$f(r) = h^{-1}(r) = \frac{r^2}{R^2} + 1 - \frac{M}{r^2}; \quad \text{where } M = \lim_{r \rightarrow 1} m(r) \quad (\text{B.4})$$

Now, consider the variation of the star's density and mass profiles as we increase ρ_0 . This is

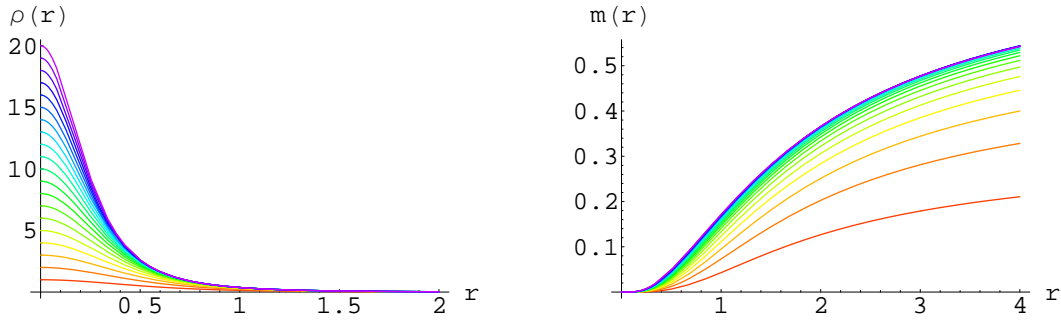


Fig. 17: Density profile, and corresponding mass profile, for a star with various values of ρ_0 (which can be read off from values of $\rho(r=0)$).

plotted in Fig.17. We see that as the star's total "extent" does not seem to change much with ρ_0 (the star is always confined within a size of order the AdS radius. This is of course due to the confining potential of the AdS geometry. Now, if the total mass could be made arbitrarily large, then for $M \ll 1$, the star would be confined within its own Schwarzschild radius, and should be viewed as a black hole. However, we see that while the density can be increased, the mass is bounded from above, and becomes largely independent of ρ_0 after some point. This is illustrated more clearly in Fig.18, where (a) the total mass, and (b) the fraction of

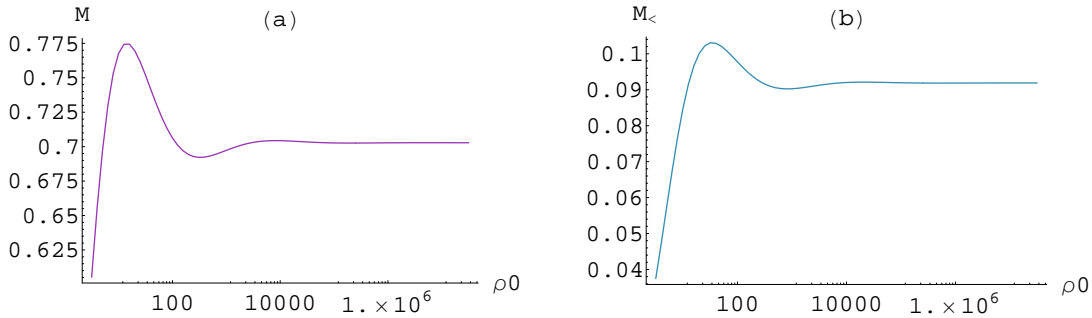


Fig. 18: Star's total mass (a), and the fraction of the star's mass confined to within this radius, plotted as a function of ρ_0 .

the star's mass confined to within its effective Schwarzschild radius is plotted as a function of ρ_0 . The left plot shows clearly that the total mass is bounded²⁷ from above by a rather small value: $M \leq 0.775R$. Curiously enough, the mass is not a monotonic function of the

²⁷In fact, this result is analogous to the similar result in the more familiar 4-dimensional, asymptotically flat static spherically symmetric spacetime, where given a fixed size R of a star (with any equation of state), the maximum possible mass such a star can attain is $M_{max} = 4R = 9$. [28]

internal density.²⁸ In fact, when examined in more detail, $M(r_0)$ appears to exhibit certain self-similarity; however we will not detour into this intriguing observation further. We also find that the effective Schwarzschild radius (i.e., what would be the Schwarzschild radius for a black hole with the total mass plotted in Fig.18a) is bounded by $r_+ = 0.716R$, so the star could at best be compared with a small Schwarzschild-AdS black hole. Most importantly, Fig.18b shows that the mass contained within the effective Schwarzschild radius is a small fraction of the total mass (less than 11%), so that the star does not approach a black hole in any regime. In other words, we should not expect to obtain behaviour characteristic of a presence of an event horizon for any value of ρ_0 .

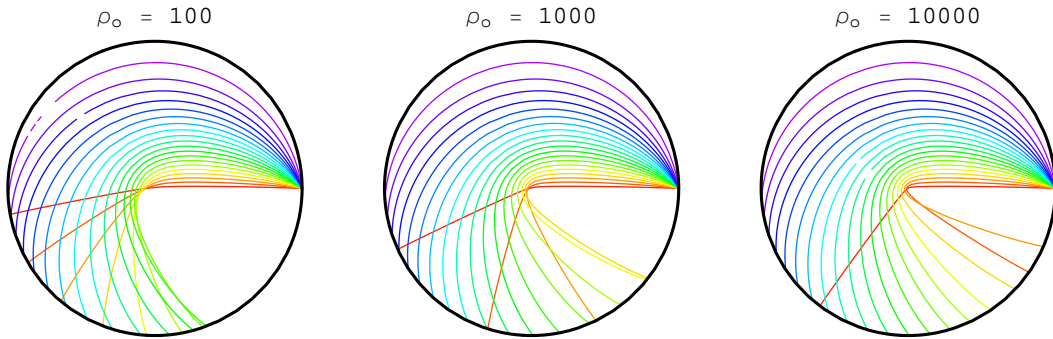


Fig. 19: Null geodesics in AdS star with three different values of ρ_0 as indicated, projected onto a constant t slice, for varying angular momentum to energy ratio.

We have seen that the star made up of a gas of radiation can never develop an event horizon, so it cannot look like a black hole, no matter how high its internal density ρ_0 . In Section 3 we have further argued for the absence of null circular orbits, and emphasized that the corresponding geodesic endpoints demonstrate a clear difference between a star and a black hole. To illustrate this further, in Fig.19 we plot the null geodesics, projected to a constant t slice, for increasing values of ρ_0 . (This is the same plot as in the left plot in Fig.4, which had $\rho_0 = 10$, redone for $\rho_0 = 100; 1000$, and 10000 , as indicated.) We see that even at very large ρ_0 , there is no null orbit. Even though the bending increases with ρ_0 , it does so ever more slowly, rather analogously to the time delay for radial geodesics (cf. Fig.3).

Appendix C : Eternal black hole in AdS

²⁸This might correspond to onset of some sort of radial instability, though there does not seem to be any obvious pathology. Correspondingly, we'll continue to include such high- ρ_0 solutions in our considerations. For the stars in 4-dimensional, asymptotically flat static spherically symmetric spacetime, [29] argued that an instability sets in at the turnover point where the mass function is non-monotone.

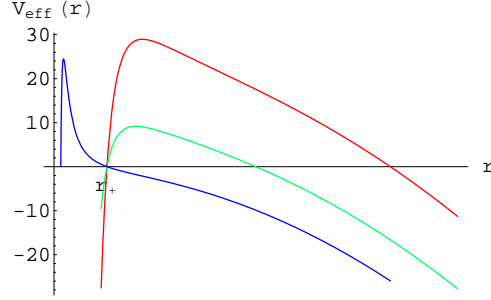


Fig. 20: Plots of $V_{\text{eff}}(r)$ for $J = 5; 3; 0.1$, which correspond to red, green and blue curves respectively. The horizon is at $r_+ = 1.78$ (for $\alpha = 1$). For $J < r_+$ (e.g. blue curve), geodesics will fall into the horizon and will not come back to the same boundary for any E . Similarly for $E > E_{\text{max}}$. E_{max} is the maximum value of V_{eff} .

We now discuss some interesting properties of spacelike geodesics in the Schwarzschild-AdS background. The geodesic equations are given in (4.4). The quantity of interest for spacelike geodesics is $(t(E; J); r'(E; J))$ which depends on both E and J .

The effective potential $V_{\text{eff}}(r)$ given in (4.5) for spacelike geodesics has two real zeros at $r = J$ and $r = r_+$, respectively. For $J < r_+$, $V_{\text{eff}}(r) < 0$ for $r > r_+$, so for any E , the spacelike geodesic will fall into the horizon²⁹ and will not come back to the same boundary. We are not interested in these geodesics. For $J > r_+$, $V_{\text{eff}}(r)$ has a maximum $V_c(J) = V_{\text{eff}}(r_m)$ at a value $r_m > r_+$ (see Fig. 20). For $E^2 > E_{\text{max}}^2(J) = V_c(J)$, the geodesic will again fall into the horizon. Thus for a spacelike geodesic to come back to the same boundary, J and E should lie in the range $J \in (r_+; \infty)$ and $E \in (0; E_{\text{max}}(J))$ for a given J .

For a fixed $J > r_+$, at $E = 0$, $(r'(0; J); t(0; J)) = (r'_c(J); 0)$. $r'_c(J)$ is a monotonic function of J . As $J \rightarrow 1$, $r'_c(J) \rightarrow \frac{2}{J} \rightarrow 0$, while as $J \rightarrow r_+$, $r'_c(J) \rightarrow 1$ logarithmically. As E varies from 0 to $E_{\text{max}}(J)$, $t(E; J)$ and $r'(E; J)$ appear to monotonically increase to infinity (see Fig. 21). As $E \rightarrow E_{\text{max}}(J)$, it can be shown that

$$t(E; J) \sim \frac{1}{s(J)} \quad r'(E; J) \rightarrow 1 \quad (\text{C } 1)$$

where $s(J)$ is given by

$$s(J) = \frac{J f(r_m)}{E_{\text{max}} r_m^2} = \frac{r}{1 + \frac{r}{r_m^4(J)}} \quad (\text{C } 2)$$

Recall that $r_m(J)$ is the maximum of $V_J(r)$. Note that $r_m(J = r_+) = r_+$ and as $J \rightarrow 1$, $r_m(J) \rightarrow (2)^{\frac{1}{2}}$. One can also check numerically that $r_m(J)$ is a monotonic function of J . From the second equality of (C 2), $s(J)$ is then a monotonic function of J decreasing from $s(J = r_+) = 2 + \frac{1}{r_+^2}$ to $s(J = 1) = 0$, where 0 was introduced in (4.6).

²⁹Subsequently it will either reach the other boundary or fall to the singularity.

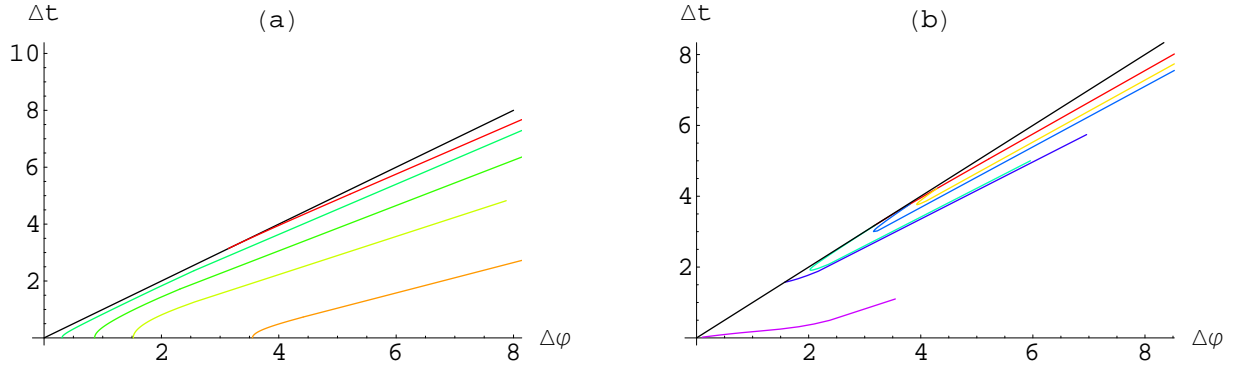


Fig. 21: The end points of various spacelike geodesics in AdS BH (with $\alpha = 1$ and $r_+ = 0.78$). Black and red line correspond to boundary and bulk null geodesics respectively as in Fig.7. (a): Various curves show how end points change as E is varied from $E = 0$ to $E_{\max}(J)$ with fixed J corresponding to $J = 0.8; 1.2; 2.2; 6.5$. The curve with larger J is farther away from the the lines corresponding to the null geodesics. Note that at $E = 0$, all lines start at real axis and as $E \rightarrow E_{\max}(q)$, t and ϕ' go to infinity. (b): Various lines describe how end points change with J for a fixed $E = J = 1.1; 1.08; 1.02; 1; 0.2$. The line with bigger value of E is closer to the lines of null geodesics. J varies from some finite J_{\min} to 1 . It is clear that as $J \rightarrow 1$ all curves approach their corresponding points on the null curve. Note that a curve with $0 < E < 1$ will end up at the origin as $J \rightarrow 1$. A curve with $E = 1$ could end up anywhere in the diagonal line between the origin and $(\phi'; t)$ depending the value of $E = J$ which should be fixed in the limit $E; J \rightarrow 1$.

From the above discussion we conclude that the end points of spacelike geodesics cover the whole region bounded by the red curve corresponding to the bulk null geodesics, the straight line from the origin to $(\phi'; t)$, and the horizontal axis in Fig.7. It is important to emphasize that ϕ' is a periodic variable, so in various figures, the fundamental region is the strip $\phi' \in (\phi'_{\min}; \phi'_{\max}]$. As a result we conclude that

1. For any end point $(\phi'; t)$ of a null geodesic (including boundary ones), there are an infinite number of spacelike geodesics ending at that point due to the periodicity of ϕ'
2. The bulk and boundary null geodesics can also share their end points for special values of t and ϕ' .

Finally let us comment on how to obtain null geodesics from spacelike geodesics by taking a limit. It is easy to see that we see that the equations for spacelike geodesics approach those of null geodesics in the limit of $E; J \rightarrow 1$ while keeping the ratio $E = J$ fixed. More explicitly, the end point of a spacelike geodesic with $0 < E < 1$ will approach the origin in the $J \rightarrow 1$ limit. A spacelike geodesic with $E = 1$ will approach a boundary null

geodesic in the limit. Its end point can be anywhere in the straight line between the origin and $(\frac{1}{2}; \frac{1}{2})$ depending the value of $E = J$ which should be fixed in the limit $E = J = 1$. A spacelike geodesic with $\frac{1}{2} < (1; 0)$ will approach a bulk null geodesic in the limit. A spacelike geodesic with $\frac{1}{2} > 0$ will not come back to the same boundary. Fig. 21 plots the end points of spacelike geodesics with $E = J$ fixed.

Appendix D : No coming back for Poincare patch

In the following we argue that for field theories formulated on $R^{d-1;1}$ there are no new light-cone singularities. As discussed in Section 2, the presence of light-cone singularities in the boundary field theory is governed by the properties of bulk null geodesics. For field theories formulated on $R^{d-1;1}$ we will show that there are no null geodesics through the bulk spacetime connecting boundary points. This implies that the only null geodesics that connect points on the boundary are those that lie entirely within the boundary and hence the nature of singularities in the correlation function is entirely determined by the boundary causal structure.

To establish the absence of null geodesics connecting boundary points through the bulk, let us consider a bulk spacetime with negative cosmological constant foliated by $R^{d-1;1}$ slices. The metric can be written in the warped-product form by picking a metric $g_{mn}(x^i)$ on the boundary and a radial coordinate r :

$$ds^2 = e^{2A(r)} g_{mn} dx^m dx^n + dr^2 \quad (D.1)$$

For this geometry one can write down the geodesic equations as

$$\begin{aligned} \ddot{r} + e^{2A(r)} g_{mn} \dot{x}^m \dot{x}^n &= 0; \\ r - A'(r) e^{2A(r)} g_{mn} \dot{x}^m \dot{x}^n &= 0 \end{aligned} \quad (D.2)$$

with $\dot{}$ being $\dot{}; 0$ for spacelike, timelike and null geodesics, respectively. By eliminating the boundary directions we can write an effective classical particle in a potential equation for the motion in the radial direction:

$$r + A'(r) (\dot{r}^2) = 0 \quad (D.3)$$

The issue of whether geodesics emanating from the boundary into the bulk turn around, can now be analyzed simply in the effective problem for the radial motion (D.3). For the case of null geodesics which we are especially interested in the first integral from (D.2) gives:

$$\dot{r} = \frac{C}{e^{A(r)}} \quad (D.4)$$

implying that $A(r) \neq 1$ for the geodesic to turn around (since $r = r_+$ by definition at the turn around point).

However, $A(r)$ cannot diverge to 1 (the energy condition on the stress tensor require that $A^0(r)$ be a monotonically decreasing function [30]). This effectively implies that $A(r)$ decreases from 1 at the AdS boundary where the field theory is formulated. Physically divergence of $A(r)$ would look like we have second timelike boundary in the geometry which again is disallowed by the null geodesic convergence condition in spacetimes where matter sources respect the null energy condition.

Appendix E : Collapsing shell in AdS

In Section 5 we derived a scaling formula for t_0 as a function of $t = t_h - t_f$ using a ray tracing calculation. The exponential relation is given in (5.6) and intuitively we can imagine this arising from the red-shift in the vicinity of the horizon. We now proceed to derive this result more explicitly, by finding actual radial null geodesics in the collapse background. In this Appendix we constrain ourselves to the sharp shell cleanly separating AdS and Schwarzschild-AdS; in Appendix F we consider the more general smeared shell collapse modeled by a Vaidya spacetime and also extend our analysis to non-radial geodesics.

Consider the set-up as sketched in Fig.8. There are two interesting limits to consider as discussed in Section 5.3. In particular, we wish to obtain the leading behaviour both as $t_i \rightarrow t_h$ and as $t_i \rightarrow t_s$, as indicated in Fig.12a and b, respectively. In fact, in order to derive both (5.6) and the scaling exponent introduced in Section 5.3, we will find the full exact expression for t_0 in terms of t_i and the parameters t_s and r_+ describing the shell. It is interesting to examine the geodesic behavior both in $d = 3$ and in $d = 5$. The distinction of course is engendered by the fact that the BTZ black hole in $d = 3$ being an orbifold of AdS_3 is a simpler geometry. On the other hand, the physics of the type III geodesics of Fig.8b is different is quite different since spacelike geodesics do not bounce off the BTZ singularity, so we can meaningfully consider only the $t_i \rightarrow t_h$ scaling.

The strategy for calculating radial null geodesics will be to write the geodesics in the different coordinate patches (such that in each patch we can use the metric of the form in (5.1)), and then patch them together using the fact that both the geodesics and the shell are null. The three regions of interest are depicted in Fig.12c, and correspond to

1. pure AdS (before/inside the shell)
2. Schwarzschild-AdS, outside the horizon (outside the shell)
3. Schwarzschild-AdS, inside the horizon (but still outside the shell)

E.1 $d = 3$

As a warm-up, let us first focus on $d = 3$. For simplicity, we use the metric (5.1) with $f(r) = r^2 + 1$ in region 1, and $f(r) = r^2 - r_+^2$ in regions 2 and 3. We will write the expressions for geodesics in 3 distinct regions (even though in 3 dimensions, region 3 is not so relevant since radial spacelike geodesics in BTZ do not bounce off the singularity). Calculating the geodesics as before, we have for pure AdS:

$$t_{\text{AdS}}(r) = t_0 + \tan^{-1} r - \tan^{-1} r_0 \quad (\text{E.1})$$

and for BTZ:

$$\begin{aligned} t_{\text{BTZ}}(r) &= t_0 + \frac{1}{r_+} \tanh^{-1} \frac{r}{r_+} - \tanh^{-1} \frac{r_0}{r_+} && \text{inside} \\ &= t_0 + \frac{1}{2r_+} \ln \frac{r+r_+}{r-r_+} - \frac{r_0+r_+}{r_0-r_+} && \text{outside} \end{aligned} \quad (\text{E.2})$$

where we denote the initial conditions by $t(r_0) = t_0$. We can now patch these together to see when a geodesic starting at $t = t_i; r = 1$ re-emerges back out to $r = 1$. Denoting this time t_0 , we can express t_0 in terms of t_i , t_s , and r_+ , obtaining:

$$t_0 = t_s + \frac{1}{r_+} \ln \frac{\tan(\frac{t_s - t_i}{2}) + r_+}{\tan(\frac{t_s - t_i}{2}) - r_+} \quad \text{if } t_0 < t_h \quad (\text{E.3})$$

Matching where the shell intersects the horizon, we can relate t_s to t_h as follows:

$$t_s = t_h + 2 \tan^{-1} r_+ \quad (\text{E.4})$$

Finally, substituting (E.4) into (E.3) and expanding for small t , we obtain the scaling behaviour

$$t_0 - \frac{1}{r_+} \ln |t_j - t_i| \approx -t \quad e^{r_+ t_0} = e^{-t_0} \quad \text{as } t_0 \rightarrow 1 \quad (\text{E.5})$$

where $\kappa = r_+$ is the surface gravity of the BTZ black hole.

Unfortunately, in this set-up we can only answer the first part of the questions raised in Section 5.3: as $t \rightarrow 0$, t_0 diverges logarithmically with the coefficient given by the black hole temperature, as one would naively expect. To see the other scalings, $t_i \rightarrow t_h^+$ and $t_i \rightarrow t_s$, discussed in Section 5.3, we need to go to higher dimensions.³⁰

³⁰If we nevertheless ignore the fact that spacelike geodesics do not bounce off the singularity, and consider the two null geodesics meeting at the singularity, then we would expect to find 1) the same scaling behaviour (same coefficient) as in (E.5) for $t_i > t_h$, and 2) $(t_s - t_i) \sim (t_0 - t_s)$ (i.e. $\kappa = 1$).

E.2 $d = 5$

Now let us consider $d = 5$. Whereas the time-radius relation for radial geodesics is independent of the dimension in pure AdS, we have a more complicated relation $t(r)$ for the black hole geometry than in the BTZ case. Writing

$$t(r) = t(r_0) + \int_{r_0}^r \frac{dr}{f(r)} \quad (\text{E.6})$$

and rewriting the metric function outside the shell as

$$f(r) = \frac{(r^2 + \frac{2}{r_+}) (r^2 - \frac{2}{r_+})}{r^2} \quad (\text{E.7})$$

where $\frac{2}{r_+} = 1 + \frac{2}{r_+^2}$, we can express the indefinite integral pertaining to outside and inside horizon regions respectively as

$$\int \frac{dr}{f(r)} = \frac{1}{r_+} + \tan^{-1} \frac{r}{r_+} + r_+ \tanh^{-1} \frac{r}{r_+} \quad \text{for } r > r_+ \quad (\text{E.8})$$

$$\int \frac{dr}{f(r)} = \frac{1}{r_+} + \tan^{-1} \frac{r}{r_+} - r_+ \tanh^{-1} \frac{r}{r_+} \quad \text{for } r < r_+ \quad (\text{E.9})$$

where $\frac{2}{r_+} = \frac{1 + 2r_+^2}{r_+}$ is the surface gravity of the black hole. For a geodesic crossing the horizon, the indefinite contribution from the coordinate singularity cancels out, so if $r_1 > r_+$ and $r_2 < r_+$, say, we would obtain

$$t_{\text{SAdS}}(r_2) = t_{\text{SAdS}}(r_1) + \frac{1}{r_+} + \tan^{-1} \frac{r}{r_+} \Big|_{r_1}^{r_2} + r_+ \tanh^{-1} \frac{r}{r_+} - r_+ \tanh^{-1} \frac{r_2}{r_+} \quad (\text{E.10})$$

Applying this to the geodesics of type II and III in Fig.12a, we obtain the full exact expression for t_0 in terms of t_s , the parameters specifying the black hole, and the radius of where the shell crosses our geodesic r_c :

$$t_0 = t_s + \frac{2}{r_+} + \frac{1}{2} + \tan^{-1} \frac{r_c}{r_+} + r_+ \tanh^{-1} \frac{r_c}{r_+} \quad \text{for geod: II} \quad (\text{E.11})$$

$$t_0 = t_s + \frac{2}{r_+} + \tan^{-1} \frac{r_c}{r_+} + r_+ \tanh^{-1} \frac{r_c}{r_+} \quad \text{for geod: III} \quad (\text{E.12})$$

where (in both cases) the crossing radius is given by

$$r_c = \tan \frac{t_s - t_h}{2} \quad (\text{E.13})$$

and the time of the shell is related to the time of horizon formation by

$$t_s = t_h + 2 \tan^{-1} r_+ \quad (\text{E.14})$$

We can easily expand this out for small t_j to check that in both cases

$$j t_j e^{-t_0} \approx t_0 \frac{1}{j t_j} : \quad (\text{E } 15)$$

This is again consistent with our expectations (5.6), and indeed of the same form as the result obtained for the 3-dimensional case.

Finally, we can also use expression (E.12) to consider the case of Fig.12b. In particular, if we let $t_s = t_j + \epsilon$, then expanding $t_s = t_j + \epsilon$ to third order in ϵ , we find that

$$t_0 = t_j + \frac{1}{12 r_+^2} \epsilon^3 : \quad (\text{E } 16)$$

This in particular implies that the scaling parameter introduced in Section 5.3 is 3 for black hole formation in $d = 5$. Intriguingly, we can generalize this to d dimensions: For d -dimensional collapse spacetime, $\epsilon = d - 2$.

Appendix F : Smeared shell in AdS and non-radial geodesics

In Appendix E, we have considered radial null geodesics in the collapsing null shell geometry. In particular, we calculated t_0 as a function of t_i and the shell parameters. As discussed in Section 5, being able to read off the value of t_i for which t_0 diverges from the gauge theory correlators, we can automatically determine the horizon formation time t_h ($= t_i$). Here we wish to extend this analysis in two directions. First, we want to consider a more general (and physically more realistic) background corresponding to a smeared shell. Second, we want to analyze non-radial geodesics, as motivated in Section 5. To that end, we will discuss general null geodesics in Vaidya-AdS spacetime.

F.1 Vaidya for AdS

Consider the stress tensor for a spherical null gas

$$T_{vv} = h(r;v) \quad (\text{F } 1)$$

The metric can be written as

$$ds^2 = -f(r;v) dv^2 + 2 dv dr + r^2 d\Omega_{d-2}^2 \quad (\text{F } 2)$$

with

$$f(r;v) = r^2 + 1 - \frac{m(v)}{r^2} \quad (\text{F } 3)$$

The covariant conservation $r \cdot T = 0$ of T implies that³¹

$$h(r;v) = \frac{1}{r^3} q(v) \quad (\text{F.4})$$

The Einstein equations now reduce to (with $\mu = 6$)

$$m'(v) = \frac{2}{3} q(v) \quad (\text{F.5})$$

For the sharp shell we take $q(v)$ has the form of a delta function, i.e.,

$$m(v) = 0 \quad v < v_0 \quad (\text{F.6})$$

$$= \quad v > v_0 \quad (\text{F.7})$$

with $q(v) = \frac{3}{2} \delta(v - v_0)$. Note that in this case the v -dependence disappears before and after the shell; the spacetime (F.2) is static in both regions (but not globally static because of the shell), written in ingoing coordinates,

$$v = t + z; \quad dz = \frac{dr}{f} \quad (\text{F.8})$$

F.2 Null geodesics

Let us now consider null geodesics in the background (F.2). Writing the second-order geodesic equation (in the equatorial plane) directly yields

$$\begin{aligned} v + \frac{1}{2} \partial_r f(r;v) \underline{v}^2 - r'^2 &= 0 \\ r \frac{1}{2} [\partial_v f(r;v) + f(r;v) \partial_r f(r;v)] \underline{v}^2 - r f(r;v) r'^2 &= 0 \\ r' + \frac{2}{r} r' \underline{v} &= 0 \end{aligned} \quad (\text{F.9})$$

For any given $f(r;v)$, we can solve these numerically to find any geodesic through the bulk. The function $f(r;v)$ with which we choose to model the smeared shell in Section 5 is

$$f(r;v) = r^2 + 1 - \frac{1 + \tanh \frac{v}{v_s}}{2} \quad (\text{F.10})$$

which smoothly interpolates between AdS at $v \ll -1$ and Schwarzschild-AdS as $v \gg +1$. In particular, the shell is inserted at³² $v = 0 = t_s + z = 2$, and has 'thickness' v_s . This provides a convenient regulator of the thin shell collapse, since as $v_s \rightarrow 0$, we recover the collapse spacetime (5.1) written in ingoing coordinates.

³¹Note that $\frac{v}{r} = \frac{r}{r} = 0$.

³²Since both AdS and Schwarzschild-AdS geometries are static, we can WLOG set the time t_s of the shell's creation on the boundary; for convenience we choose $t_s = -2$.

However, to find the geodesics in the collapse spacetime, and especially to determine $t_h(\cdot)$, we can use a simpler and more elegant method, which we now indicate. The geodesics can be obtained from the following action

$$S = \int d\tau \left[\frac{1}{2} f \underline{v}^2 + \underline{v} \underline{r} + \frac{1}{2} r^2 \dot{\underline{r}}^2 \right] \quad (\text{F.11})$$

The canonical momenta are

$$J = r^2 \dot{\underline{r}}; \quad E = \frac{\partial L}{\partial \underline{v}} = \underline{r} + f \underline{v}; \quad \frac{\partial L}{\partial \underline{r}} = \underline{v} \quad (\text{F.12})$$

Note that J is conserved, while E is in general not. Note that J can be scaled to be 1 by a rescaling of τ . As before, we will denote $\underline{v} = \frac{E}{J}$ and set $J = 1$. Another first integral of the system is given by

$$\underline{r}^2 + \frac{f}{r^2} = \text{const}^2 \quad (\text{F.13})$$

The equations of motion can now be written as

$$\dot{\underline{r}} = \frac{1}{2} \frac{\partial f}{\partial \underline{v}} \underline{v}^2 \quad (\text{F.14})$$

$$\dot{\underline{v}} = \frac{1}{2} \frac{\partial f}{\partial r} \underline{v}^2 + \frac{1}{r^3} \quad (\text{F.15})$$

From the above equations we can also derive

$$\dot{r} = \frac{1}{2} \frac{\partial f}{\partial \underline{v}} \underline{v}^2 - \frac{1}{2r^2} \frac{\partial f}{\partial r} + \frac{f}{r^3} \quad (\text{F.16})$$

where we have used that

$$\underline{v} = \frac{\dot{r} + \underline{r}}{f} \quad (\text{F.17})$$

Now we apply the above equations to the Vaidya spacetime with a sharp shell, in which case

$$\frac{\partial f}{\partial \underline{v}} = \frac{1}{r^{d-3}} (\underline{v} - \underline{v}_0) \quad (\text{F.18})$$

The discontinuity of f across $\underline{v} = \underline{v}_0$ is thus given by $\Delta f = \frac{1}{r^{d-3}}$. One can readily conclude from the above equations that both \underline{r} and \underline{v} jump across $\underline{v} = \underline{v}_0$, in fact by the same amount, while $\dot{\underline{v}}$ is continuous. More explicitly we find that

$$\Delta \underline{r} = \Delta \underline{v} = \frac{1}{2r^{d-3}} \frac{\underline{v}}{\underline{v}_0} < 0 \quad (\text{F.19})$$

Let us now return to the problem of determining $t_h(\cdot)$ for the collapse geometry. Realizing that \underline{r} jumps across the shell, let us work backwards by considering what feature of the geodesics makes t_h large. The relevant spacetime to consider is Schwarzschild-AdS, wherein the geodesics follow from the potential (4.5) drawn in Fig.6. Since the top of

the potential is always outside the horizon (as follows from the discussion in Section 4, $r_m^2 = 2 = 2r_+^2 (r_+^2 + 1) > r_+^2$), the only way that a non-radial null geodesic could emerge at finite time would be to get trapped in the unstable circular orbit at the top of the effective potential. This requires

$$\dot{\phi}^2 = V_{\text{eff}}(r_m) = 1 + \frac{1}{4} \quad (\text{F } 20)$$

Knowing the $\dot{\phi}$ in the Schwarzschild-AdS part of the spacetime, we can now use the expression (F.19) for the jump in ϕ across the shell, to find what initial conditions (i.e. what $\dot{\phi}_i$ in AdS) we need to start with to achieve this $\dot{\phi}_o$. Using (F.17), (F.13), and the expression for $f(r)$ in AdS (5.2), all evaluated at some crossing radius r_x where the geodesic intersects the shell, we can reexpress (F.19) as follows:

$$\dot{\phi}_o = \dot{\phi}_i \frac{1 + \frac{q}{2} \frac{r_+^2 + 1}{r_x^2}}{2r_x^2 (r_x^2 + 1)} \quad (\text{F } 21)$$

Finally, we can express the crossing radius r_x in terms of the initial time t_i by following the geodesic with parameter $\dot{\phi}_i$ from r_x back to its starting point on the boundary at t_i . This is given by

$$t_o - t_i = \tan^{-1} r_x + \tan^{-1} \frac{p}{(\dot{\phi}_i^2 - 1) r_x^2 - 1} \quad (\text{F } 22)$$

Note that t_i should be viewed as a function of $\dot{\phi}_i$, and for $t_o \rightarrow 1$, this is nothing but $t_h(\dot{\phi}_i)$ of Section 5, where we have been using $\dot{\phi}_i$.

Hence, to find $t_h(\dot{\phi}_i)$, we can solve the system of equations (F.20), (F.21), and (F.22). We first solve (F.20) and (F.21) for the crossing radius $r_x(\dot{\phi}_i)$, and then substitute this into (F.22) to find $t_h(\dot{\phi}_i) = t_i$, as a function of $\dot{\phi}_i$ and the shell parameters, q and t_s . This determines the black curve plotted in Fig.9. Note that the radial geodesic limit ($\dot{\phi}_i \rightarrow 1$) is continuous, despite the fact that only the radial geodesic can truly sample the horizon formation event, since only the null outgoing radial geodesics can escape from the close vicinity of the horizon.

References

- [1] G. T. Horowitz and N. Izhaki, "Black holes, shock waves, and causality in the AdS/CFT correspondence," JHEP 02 (1999) 010, hep-th/9901012.
- [2] D. Kabat and G. Lifschytz, "Gauge theory origins of supergravity causal structure," JHEP 05 (1999) 005, hep-th/9902073.
- [3] S. Gao and R. M. Wald, "Theorems on gravitational time delay and related issues," Class. Quant. Grav. 17 (2000) 4999{5008, gr-qc/0007021.

- [4] V. E. Hubeny, M. Rangamani, and S. F. Ross, "Causal structures and holography," *JHEP* 07 (2005) 037, hep-th/0504034.
- [5] J. P. Gregory and S. F. Ross, "Looking for event horizons using UV/IR relations," *Phys. Rev. D* 63 (2001) 104023, hep-th/0012135.
- [6] L. Fidkowski, V. Hubeny, M. Kleban, and S. Shenker, "The black hole singularity in AdS/CFT," *JHEP* 02 (2004) 014, hep-th/0306170.
- [7] G. Festuccia and H. Liu, "Excursions beyond the horizon: Black hole singularities in Yang-Mills theories. I," hep-th/0506202.
- [8] J. Louko, D. Marolf, and S. F. Ross, "On geodesic propagators and black hole holography," *Phys. Rev. D* 62 (2000) 044041, hep-th/0002111.
- [9] P. Kraus, H. Ooguri, and S. Shenker, "Inside the horizon with AdS/CFT," *Phys. Rev. D* 67 (2003) 124022, hep-th/0212277.
- [10] B. Freivogel, V. Hubeny, A. Maloney, R. Myers, M. Rangamani, and S. Shenker, "Information in AdS/CFT," *JHEP* 03 (2006) 007, hep-th/0510046.
- [11] J. Hammersley, "Extracting the bulk metric from boundary information in asymptotically AdS spacetimes," hep-th/0609202.
- [12] M. Kleban, J. McGreevy, and S. D. Thomas, "Implications of bulk causality for holography in AdS," *JHEP* 03 (2004) 006, hep-th/0112229.
- [13] G. T. Horowitz and V. E. Hubeny, "CFT description of small objects in AdS," *JHEP* 10 (2000) 027, hep-th/0009051.
- [14] H. Lin, O. Lunin, and J. Maldacena, "Bubbling AdS space and 1/2 BPS geometries," *JHEP* 10 (2004) 025, hep-th/0409174.
- [15] S. D. Mathur, "The fuzzball proposal for black holes: An elementary review," *Fortsch. Phys.* 53 (2005) 793{827, hep-th/0502050.
- [16] S. D. Mathur, "The quantum structure of black holes," hep-th/0510180.
- [17] U. H. Danielsson, E. Keski-Vakkuri, and M. Kuczenski, "Spherically collapsing matter in AdS, holography, and shellons," *Nucl. Phys. B* 563 (1999) 279{292, hep-th/9905227.
- [18] S. B. Giddings and S. F. Ross, "D3-brane shells to black branes on the Coulomb branch," *Phys. Rev. D* 61 (2000) 024036, hep-th/9907204.
- [19] S. B. Giddings and A. Nudelman, "Gravitational collapse and its boundary description in AdS," *JHEP* 02 (2002) 003, hep-th/0112099.

- [20] K. M. Aeda, M. Natsuume, and T. Okamura, "Extracting information behind the veil of horizon," hep-th/0605224.
- [21] S. W. Hawking, "Particle creation by black holes," Commun. Math. Phys. 43 (1975) 199{220.
- [22] V. Balasubramanian, V. Jejjala, and J. Simon, "The library of Babel," Int. J. Mod. Phys. D 14 (2005) 2181{2186, hep-th/0505123.
- [23] V. Balasubramanian, J. de Boer, V. Jejjala, and J. Simon, "The library of Babel: On the origin of gravitational thermodynamics," JHEP 12 (2005) 006, hep-th/0508023.
- [24] V. Balasubramanian, P. Kraus, and M. Shigemori, "Massless black holes and black rings as effective geometries of the D1-D5 system," Class. Quant. Grav. 22 (2005) 4803{4838, hep-th/0508110.
- [25] V. Balasubramanian, B. Czech, K. Larjo, and J. Simon, "Integrability vs. information loss: A simple example," hep-th/0602263.
- [26] M. W. Choptuik, "Universality and scaling in gravitational collapse of a massless scalar field," Phys. Rev. Lett. 70 (1993) 9{12.
- [27] D. N. Page and K. C. Phillips, "Selfgravitating radiation in anti-de Sitter space," GRG (1985).
- [28] R. M. Wald, "General relativity," Chicago, USA: Univ. Pr. (1984) 491p.
- [29] R. Sorkin, "A criterion for the onset of instability at a turning point," Astrophys. J. 249 (1981) 254{257.
- [30] D. Z. Freedman, S. S. Gubser, K. Pilch, and N. P. Warner, "Renormalization group flows from holography supersymmetry and a c-theorem," Adv. Theor. Math. Phys. 3 (1999) 363{417, hep-th/9904017.